NASA TECHNICAL NOTE

NASA TN D-7591

NASA TN D-7591

SECONDARY ELECTRON BACKGROUND PRODUCED BY HEAVY NUCLEI IN A MULTIWIRE PROPORTIONAL COUNTER HODOSCOPE

by S. H. Morgan, Jr., J. W. Watts, Jr., H. Schwille, and U. Pollvogt

George C. Marshall Space Flight Center
Marshall Space Flight Center, Ala. 35812

NATIONAL AERONAUTICS AND SPACE ADMINISTRATION • WASHINGTON, D. C. • FEBRUARY 1974

TECHNICAL REPORT STANDARD TITLE PAGE

1. REPORT NO.	2. GOVERNMENT ACCESSION NO.	3. RECIPIENT'S CATALOG NO.
NASA TN D- 7591		

4. TITLE AND SUBTITLE
Secondary Electron Background Produced by Heavy Nuclei in a Multiwire Proportional Counter Hodoscope

5. REPORT DATE
February 1974

6. PERFORMING ORGANIZATION CODE

7. AUTHOR(S)
S. H. Morgan, Jr., J. W. Watts, Jr., H. Schwille*, and U. Pollvogt†

8. PERFORMING ORGANIZATION REPORT #
M-462

9. PERFORMING ORGANIZATION NAME AND ADDRESS
George C. Marshall Space Flight Center
Marshall Space Flight Center, Alabama 35812

10. WORK UNIT NO.

11. CONTRACT OR GRANT NO.

13. TYPE OF REPORT & PERIOD COVERED

12. SPONSORING AGENCY NAME AND ADDRESS
National Aeronautics and Space Administration
Washington, D.C. 20546

14. SPONSORING AGENCY CODE

15. SUPPLEMENTARY NOTES
Prepared by Space Sciences Laboratory, Science and Engineering Directorate
* Formerly at Space Sciences Laboratory
† Current Address: TRW Systems, Inc., Redondo Beach, Calif. 90278

16. ABSTRACT

The secondary electron background produced by heavy nuclei in a multiwire proportional counter hodoscope is calculated using both a simplified and a more complete Monte Carlo model. These results are compared with experimental data from a small multiwire proportional counter hodoscope operated in a 530 MeV/nucleon accelerator beam of nitrogen nuclei. Estimates of the secondary electron background produced by heavy relativistic nuclei are presented along with the detailed results from calculations of energy deposition in the hodoscope counter cells.

17. KEY WORDS	18. DISTRIBUTION STATEMENT
	Distribution Category: 29 Cat.29

19. SECURITY CLASSIF. (of this report)	20. SECURITY CLASSIF. (of this page)	21. NO. OF PAGES	22. PRICE
Unclassified	Unclassified	46 46	

ACKNOWLEDGMENT

The authors express their appreciation to Dr. T. A. Parnell for many valuable discussions and suggestions during the preparation of this report.

TABLE OF CONTENTS

LIST OF ILLUSTRATIONS

LIST OF ILLUSTRATIONS (Continued)

LIST OF ILLUSTRATIONS (Concluded)

SECONDARY ELECTRON BACKGROUND PRODUCED BY HEAVY NUCLEI IN A MULTIWIRE PROPORTIONAL COUNTER HODOSCOPE

SECTION I. INTRODUCTION

The energy deposited by a heavy ion passing through a detector depends linearly upon the pathlength of the ion. Therefore, among parameters that one must know to determine the charge of the primary ion is the trajectory. Some of the devices used as a hodoscope for this purpose are multiwire proportional counters (MWPC), spark chambers, and crossed scintillator strips [1]. In all cases a number of secondary electrons are produced by the interaction of the primary ion with the detector material. Thus, one must be able to obtain the trajectory in the presence of a background of secondary electrons. Furthermore, since the number of secondary electrons varies approximately as the square of the charge of the primary ion [2,3], this background becomes increasingly important for heavy ions.

This report presents a study based upon a simplified Monte Carlo simulation of the influence of the secondary electron background on a MWPC hodoscope. The results of this investigation are compared with results from an experiment performed by two of the authors using a small MWPC exposed in a 530 MeV/nucleon accelerator beam of nitrogen nuclei. Finally, data from a more detailed and accurate Monte Carlo model are presented both as a test of the limitations of the simplified model and to provide data that may be useful in performing other experiments in which hodoscopes for highly charged particles are used.

SECTION II. THEORY

A. Ionization and Excitation Energy Loss

The primary processes by which a relativistic heavy charged particle loses energy as it traverses a sparse medium are ionization and excitation of the atoms in the medium. For these processes the average energy loss in units of MeV-cm^2/g of a heavy particle with charge Ze and velocity βc traversing X g/cm^2 of material with atomic number Z′ and atomic weight A is given by the well-known Bethe-Bloch [3] equation

$$-\frac{dE}{dX} = 2\,\xi\,X\,[\ln(E_m/I) - \beta^2 - k/Z' - \delta/2] \qquad (1)$$

where

$\xi = 0.1535\ (Z/\beta)^2\ Z'/A$

I = mean excitation energy of the medium

E_m = maximum energy transferrable to an atomic electron (assumed to be initially free) of the medium by a heavy charged particle ($E_m \approx 2m_e c^2\ \gamma^2\ \beta^2$)

$\gamma = (1 - \beta^2)^{-1/2}$

m_e = electron rest mass

k/Z' = shell correction factor

δ = density effect correction

(The latter two corrections are not significant for conditions considered in this report and will be omitted. See, for example, Reference 4.)

The Bethe-Bloch equation may be divided into two parts depending upon the amount of energy transferred in a collision [5]. The dividing energy η is chosen as an energy above which the atomic electron binding energy may be neglected. The value of η used in the following calculations was 10^4eV [3,5]. "Distant" collisions are those in which an energy less than η is transferred, and "close" collisions are those in which an energy between η and E_m is transferred to an atomic electron. Most of the energy is lost through the numerous distant collisions, which have the effect of raising the atomic electrons to higher energy states. For close collisions, if sufficient energy is transferred, some of the atoms will be ionized, resulting in secondary electrons moving through the medium. (Throughout the remainder of this report, unless otherwise indicated, all electrons referred to will be secondary electrons, and the word secondary will be omitted.)

The average ionization and excitation energy loss will not, in general, be the same as the most probable energy loss. Since the energy transferred in an individual collision is an independent event, it will vary. The actual energy loss will obey a distribution depending upon the charge and velocity of the incident particle, the medium through which it passes, and the thickness of the medium. Vavilov [6,7] has developed such a

distribution function by solving the transport equation that describes this function. The Vavilov distribution for 530 MeV/nucleon nitrogen nuclei traversing 28 cm of argon at 1 atmosphere is shown in Figure 1, where the average energy loss from equation (1) is indicated by $\bar{\epsilon}$. Note that the distribution is asymmetric with a high energy tail corresponding to those rare events where a large amount of energy is transferred.

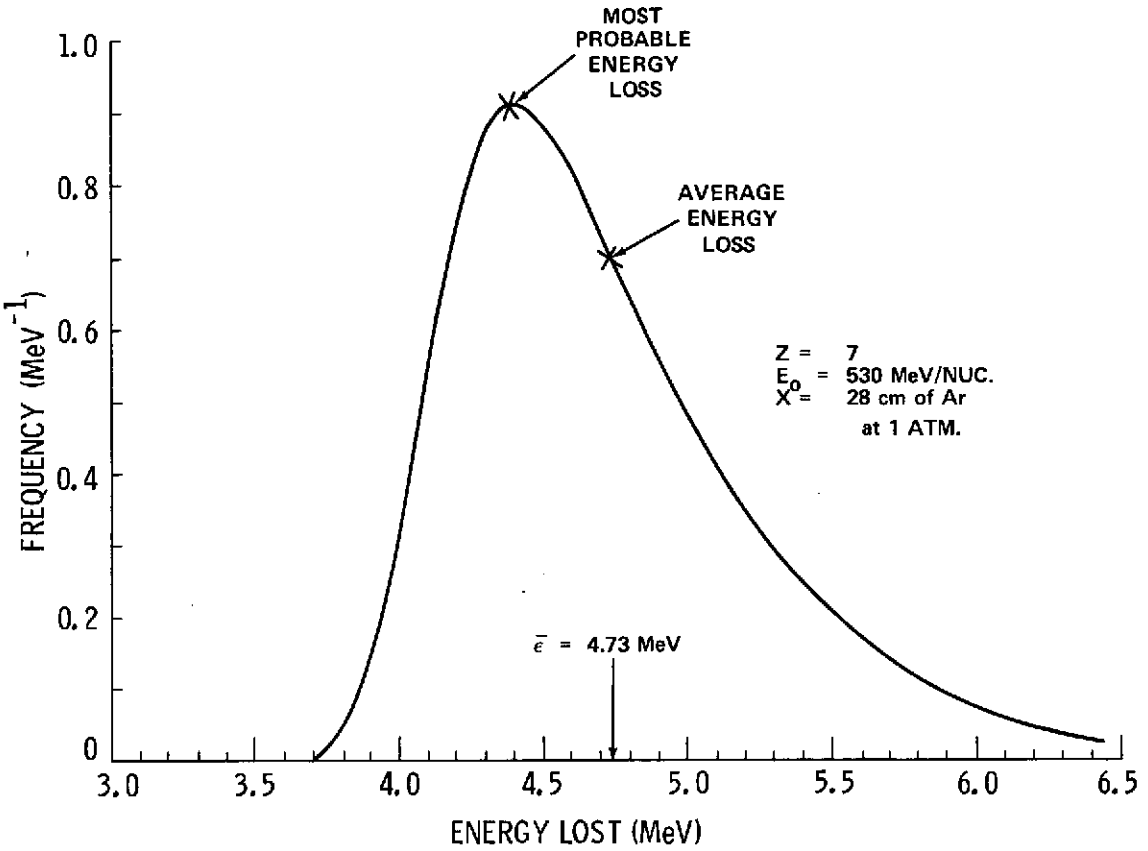

Figure 1. Vavilov distribution for 530 MeV/nucleon nitrogen nuclei traversing 28 cm of argon.

There is usually a difference between the amount of energy lost by a particle in a detector and the amount deposited. Most of the electrons produced in the collisions have low energies and, thus, travel only a short distance before stopping in the medium. However, a number of these may receive sufficient energy to escape the detector and will carry a portion of the energy that is lost in the detector away from the detector volume. This is especially true for a thin detector. In addition, electrons produced by the primary particle in the material adjacent to the detector may enter the detector. Therefore, most of the energy will be deposited in a core around the path of the incident particle, with lesser amounts deposited by electrons in other locations.

B. Secondary Electron Distributions

The distributions of average number, energy, range, and angle of emission of electrons produced by heavy primary nuclei are calculated below. Distributions from 530 MeV/nucleon nitrogen nuclei in a gaseous mixture of Ar (90%) + CO_2 (10%) are illustrated in Figures 2 through 6.

The average number of electrons with energies between E_1 and E_2 produced by a heavy ion traversing X g/cm^2 of material is given by:

$$\langle N \rangle = N'X \int_{E_1}^{E_2} \left(\frac{d\sigma}{dE} \right) dE \qquad (2)$$

where N' is the number of atomic electrons/cm^3 of material and $d\sigma/dE$ is the cross section for the production of an electron of energy E by a heavy charged particle [2]. If the first Born approximation,

$$\frac{d\sigma}{dE} = \xi \, (N' \, E^2)^{-1} \, (1 - \beta^2 \, E/E_m) \quad ,$$

is used, the resulting form of equation (2) is:

$$\langle N \rangle = \xi \, X \, [1/E_1 - 1/E_2 - \beta^2/E_m \ln (E_2/E_1)] \qquad (3)$$

This distribution is illustrated in Figure 2 where the average number of electrons produced per centimeter of primary ion track with energy greater than E′ is plotted as a function of E′. Note that the distribution is very steep at low energies, indicating a very high production probability for the lowest energy calculated (in this case 18 keV) and a very low probability of producing electrons with energies approaching E_m. For example, nitrogen nuclei with an energy of 530 MeV/nucleon will produce on the average only 1 electron with energy $\geq$ 200 keV in traversing 28 cm of the argon-CO_2 gas, whereas 15 are produced with energies $\geq$ 18 keV.

If Θ_δ is the angle that the electron makes with the assumed straight path of the primary, one finds from conservation of energy and momentum that

$$\cos \Theta_\delta \approx \frac{1}{\beta} \sqrt{\frac{E}{E + 2m_e c^2}} \qquad (4)$$

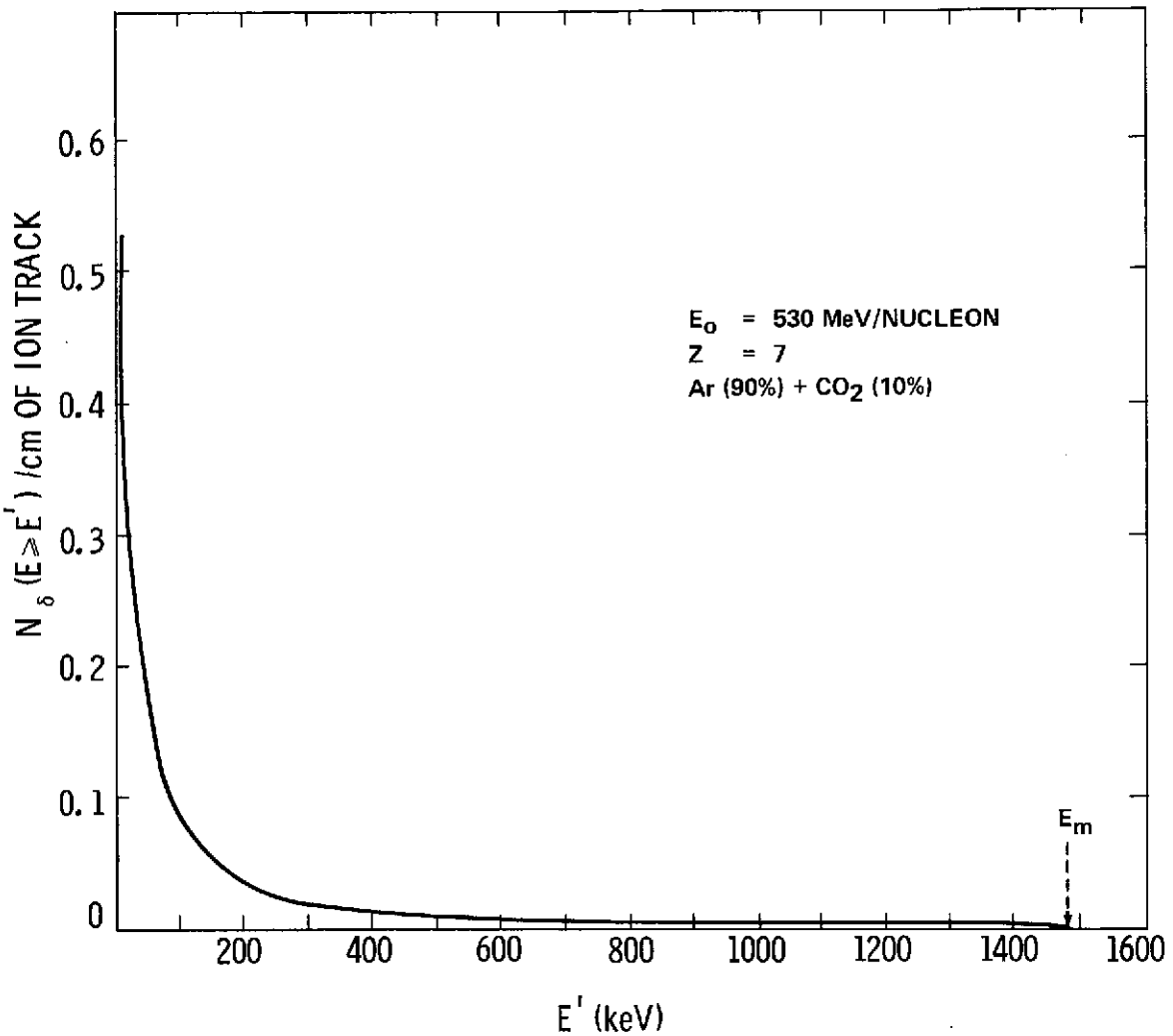

Figure 2. Average number of secondary electrons produced by 530 MeV/nucleon nitrogen nuclei versus secondary electron energy.

Figure 3 shows the angular distribution of the electrons versus Θ_δ', the angle of emission from the primary particles path. The ordinate is the average number of electrons produced per centimeter of primary particle path that are emitted at an angle less than or equal to Θ_δ'. One notes from the figure that the majority of the electrons are produced nearly normal to the path of the particle. In Figure 4 the angle of emission of an electron versus the initial electron energy is shown. One notes that in those rare cases where the electron receives a large amount of energy in a collision it is emitted in the forward direction as expected.

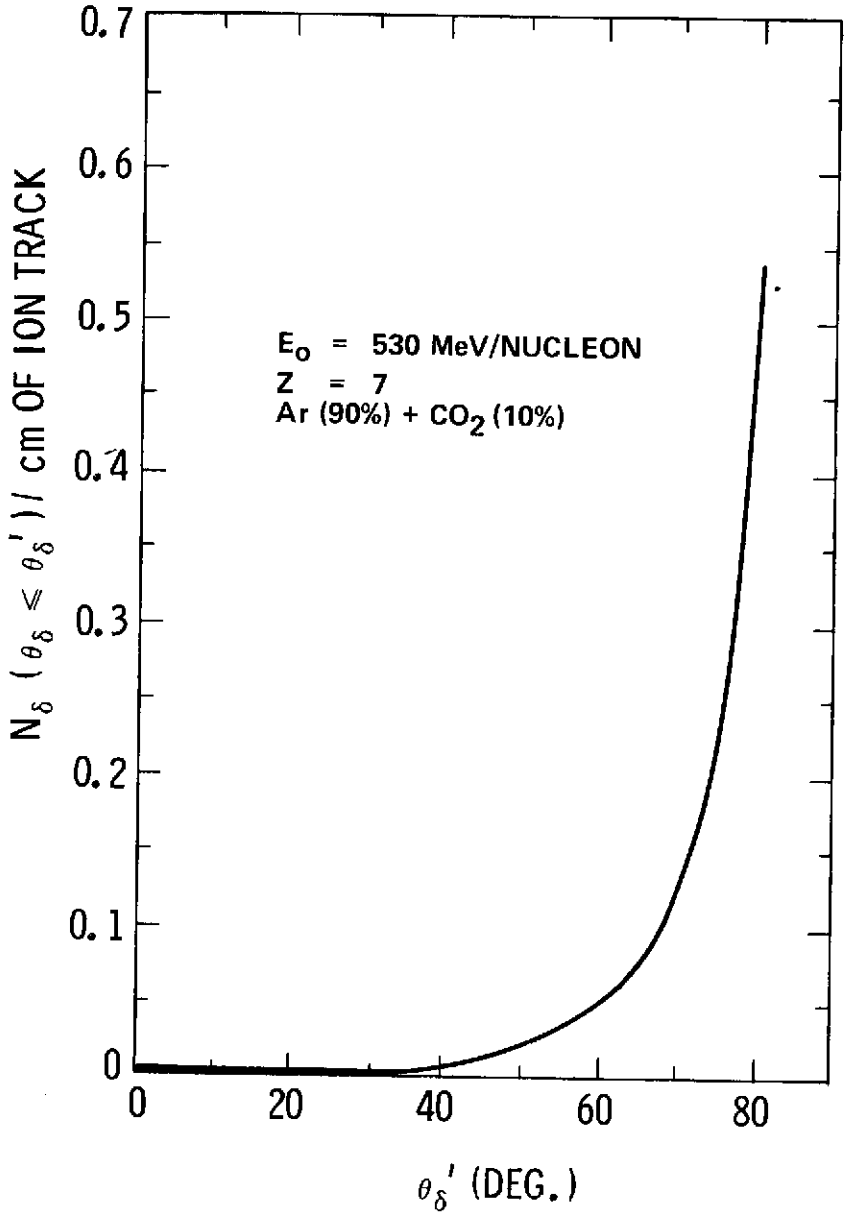

Figure 3. Angles of emission of secondary electrons produced by 530 MeV/nucleon nitrogen nuclei.

The extrapolated range of electrons, illustrated in Figure 5, is used in the calculations instead of the mean range to insure that the range predictions are conservative. This is especially desirable since the straight-ahead approximation is used in the Monte Carlo model discussed in Section II-C. The extrapolated range of an electron with energy E in units of MeV is given by [8]

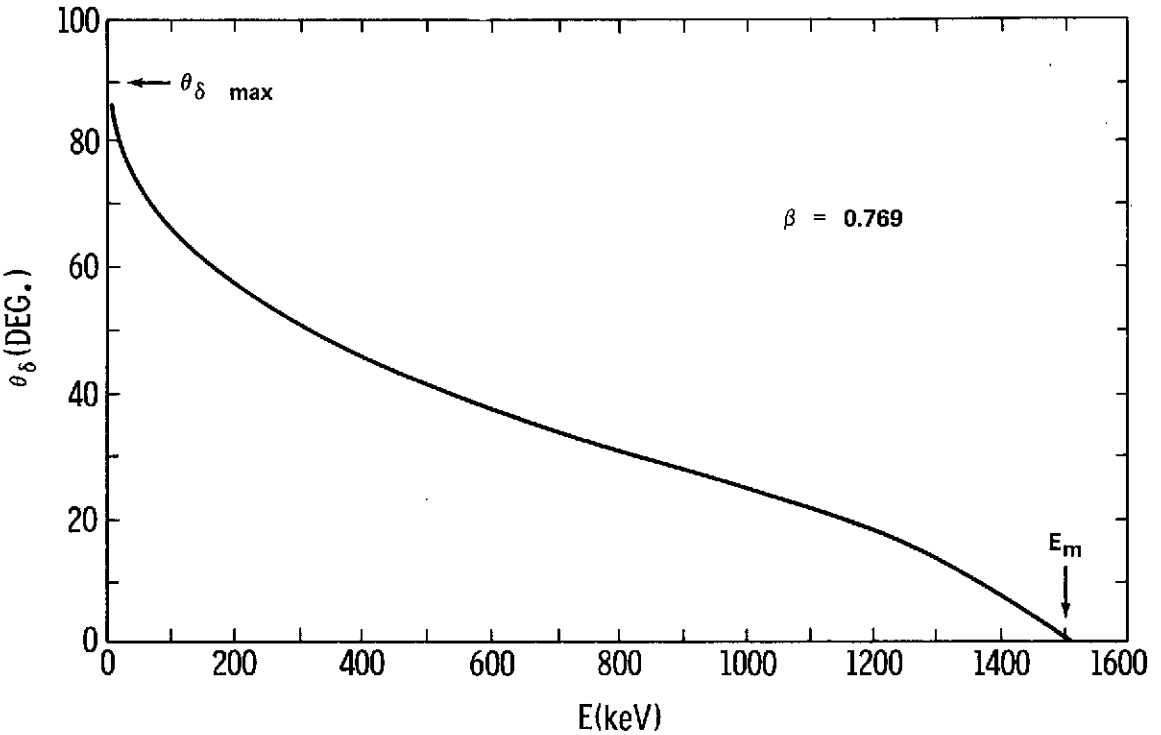

Figure 4. Angles of emission of secondary electrons as a function of electron energy.

$$R_{ex} = 0.481 \frac{A}{Z'} \left[\sqrt{\left(\frac{E}{a}\right)^2 + b^2} - b \right] g/cm^2 \quad (5)$$

where a = 1.92, b = 0.11, A is the atomic weight, and Z' is the atomic number of the medium. The electron range distribution is illustrated in Figure 6, which is similar to Figure 2 except that the abscissa is in terms of extrapolated range. This figure shows, for example, that the average number of electrons produced with ranges greater than or equal to 2 cm by the primary particle in traversing 28 cm of the gas is approximately 5.

C. Simplified Monte Carlo Simulation

Since the process under investigation is statistical in nature, an obvious approach to obtain results to compare with the experiment is Monte Carlo simulation [9]. The method used is simplified primarily in that multiple scattering of the electrons in the

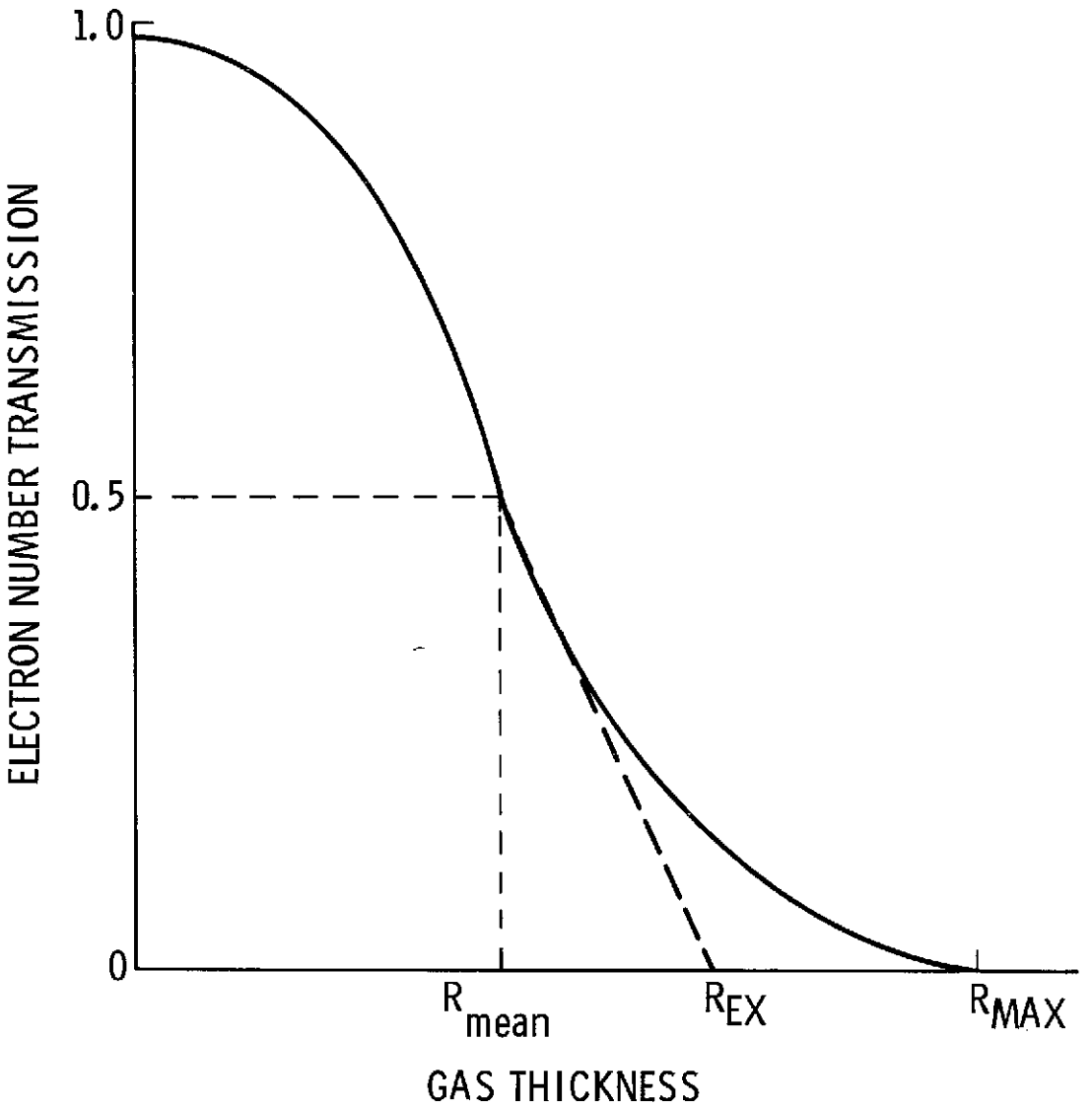

Figure 5. Illustration of extrapolated range for electrons.

detector gas is neglected. In carrying out this simulation, the following assumptions were used:

1. Heavy ions are incident normally to the detector and travel in straight-line paths through the detector.

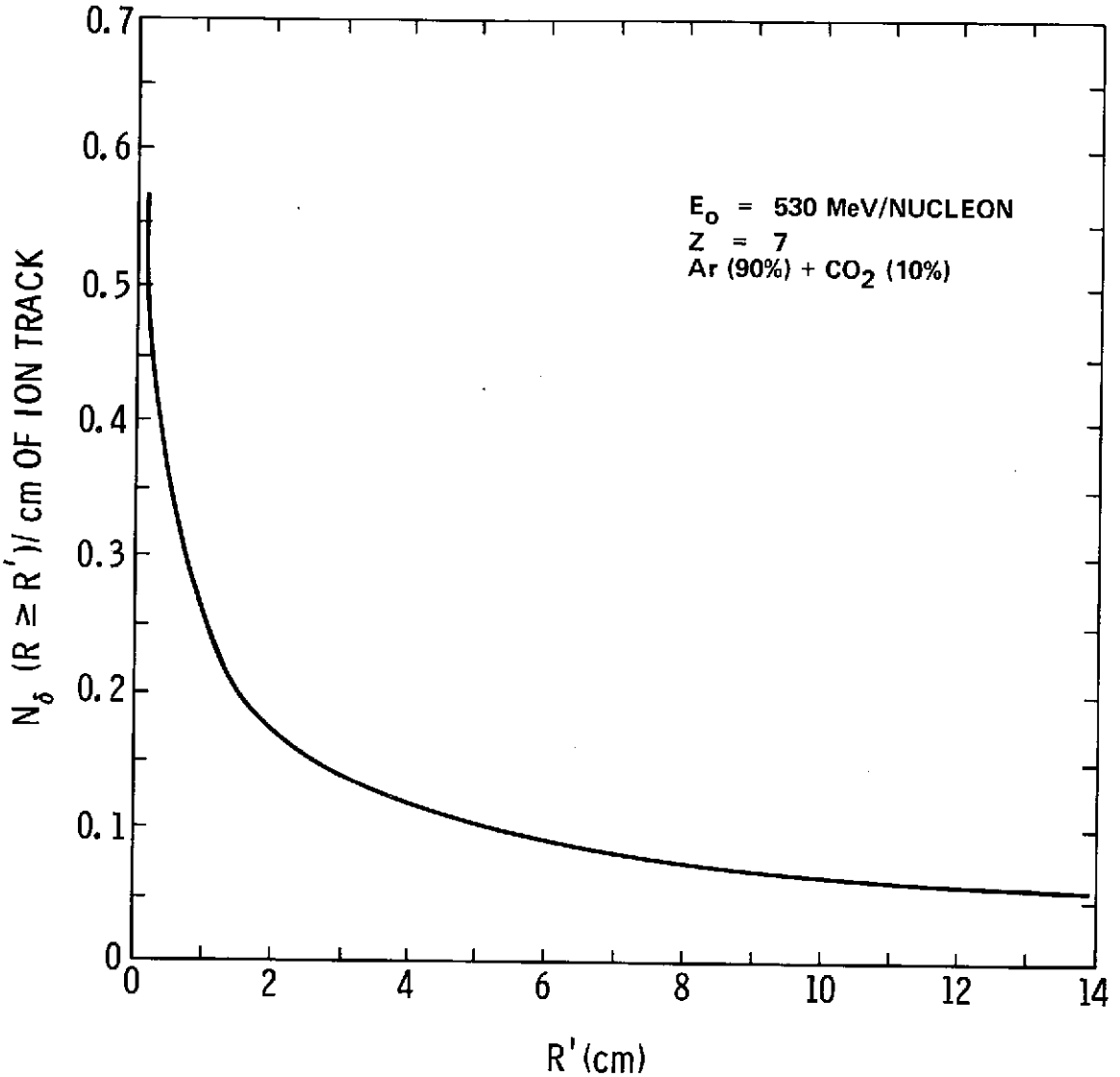

Figure 6. Average number of secondary electrons produced by 530 MeV/nucleon nitrogen nuclei versus extrapolated range.

2. The electrons produced by collisions with the detector gas travel in a straight line in the media, with range given by the empirical energy-range relationship, equation (5).

3. The minimum electron energy considered in the calculations depends upon the distance from the heavy particle track to the closest detector region of interest; i.e., the nearest MWPC anode wire.

4. The number of electrons produced obeys a Poisson distribution, with the average given by equation (3).

5. No interactions other than those with the detector gas are considered.

Using assumption 4, the probability of a primary ion producing n electrons in traveling ΔX units of its path length may be found from:

$$P(n) = \exp(-\langle N\rangle)\,\langle N\rangle^{n}/n! \tag{6}$$

where $\langle N\rangle$ is the average number of electrons produced in ΔX. However, for sampling purposes, the most convenient distribution to use is the cumulative Poisson distribution. Thus, the probability of producing as many as N electrons is given by:

$$P(n \leqslant N) = \sum_{n=1}^{N} \exp(-\langle N\rangle)\,\langle N\rangle^{n}/n! \tag{7}$$

To find N, one first chooses a random number r_1, where $0 \leqslant r_1 \leqslant 1$, and samples from the distribution given by equation (7); i.e., one solves the inequality,

$$\sum_{n=1}^{N-1} \exp(-\langle N\rangle)\,\langle N\rangle^{n}/n! \;<\; r_1 \;\leqslant\; \sum_{n=1}^{N} \exp(-\langle N\rangle)\,\langle N\rangle^{n}/n!$$

for N. This is illustrated in Figure 7, where the random number 0.7 would result in a value N = 4 for the case Z = 7, E_0 = 530 MeV/nucleon, and X = 7 cm of argon.

After the number of electrons produced in distance ΔX by the primary is found, one next obtains the energy E′ of an individual electron by sampling from the normalized cumulative distribution F.

$$F = P(E' \geqslant E \geqslant E_1)/P(E_2 \geqslant E \geqslant E_1)$$

$$= N' \int_{E_1}^{E'} \left(\frac{d\sigma}{dE}\right) dE \Big/ N' \int_{E_1}^{E_2} \left(\frac{d\sigma}{dE}\right) dE$$

$$= \frac{N'}{\langle N \rangle} \int_{E_1}^{E'_0} \left(\frac{d\sigma}{dE}\right) dE$$

or, using the first Born approximation for $d\sigma/dE$,

$$F = \frac{\xi}{\langle N \rangle} \left[\frac{1}{E_1} - \frac{1}{E'} - \frac{\beta^2}{E_m} \ln\left(\frac{E'}{E_1}\right)\right] \tag{8}$$

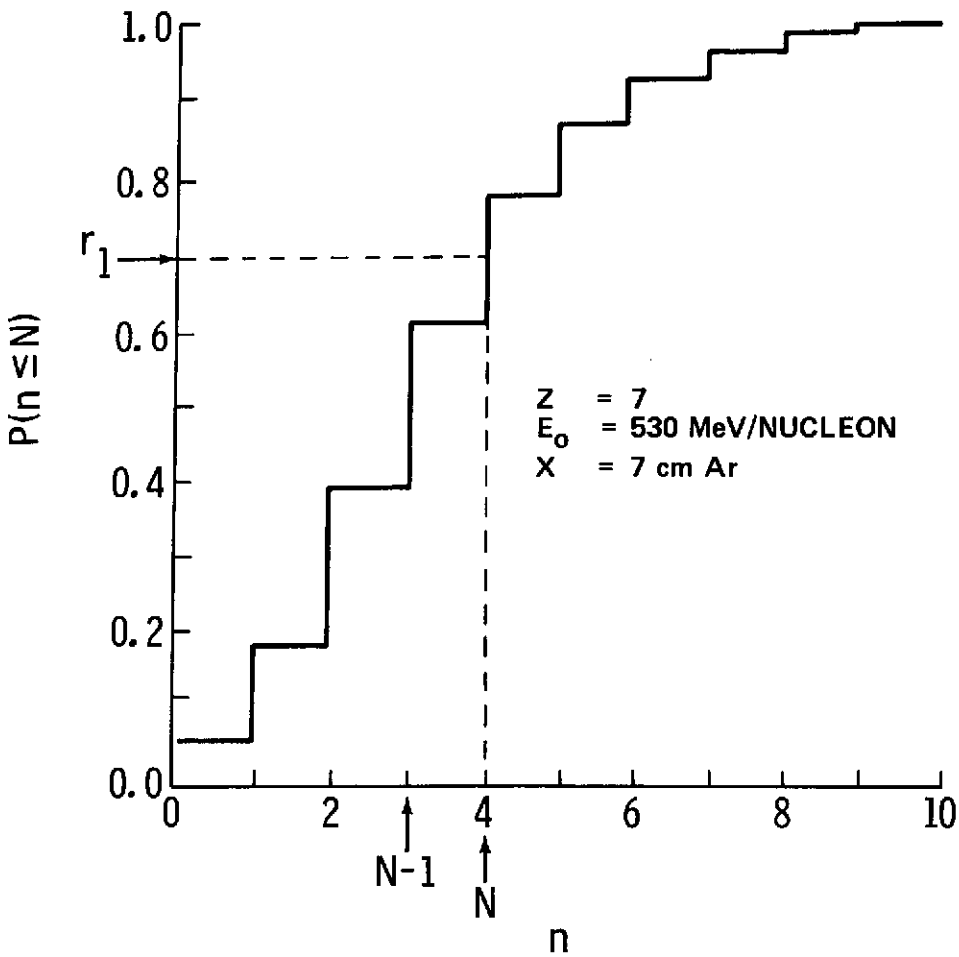

Figure 7. Sampling from cumulative Poisson distribution.

The procedure one uses is to first choose a random number $0 \leqslant r_2 \leqslant 1$ and set $r_2 = F$ in equation (8); then

$$E' = \frac{1}{E_1} + \frac{\beta^2}{E_m} \ln (E_1) - \frac{\beta^2}{E_m} \ln (E') - n_2 \frac{\langle N \rangle}{\xi} \qquad (9)$$

This is a transcendental equation in E' which may be solved by a simple iterative calculation.

Using the energy E' in equation (9), one finds the range of the electron and from the electron energy and the velocity of the primary ion obtains the angle of emission from equation (4).

To obtain the azimuthal angle of emission, ϕ, one notes that there are no preferred azimuthal directions of electron emission. Therefore, assuming that ϕ occurs randomly between 0 and 2π, one sets

$$\phi = 2\pi r_3 \quad ,$$

where, again, $0 \leqslant r_3 \leqslant 1$.

A computer code was developed to carry out the previous calculations and graphically display the results. The code performs the simulation in the following sequence:

1. Calculate the average number of electrons produced $\langle N \rangle$ for increment ΔX of the incident particle path from equation (3).

2. Using the above value for $\langle N \rangle$, sample from the cumulative Poisson distribution as illustrated by Figure 7 to obtain the number N of electrons with energies between E_1 and E_m that are produced as the heavy ion traverses distance ΔX.

3. Use equation (9) to sample from the electron energy distribution to obtain the energy for each of the above N electrons.

4. Calculate the range and angle of emission for each electron using equations (5) and (4), respectively.

5. Follow the electrons throughout their path to determine whether they enter a sensitive volume about a given wire. This volume is an adjustable parameter (Section III-B). These data are stored for later analysis.

The code next determines the energy loss incurred by the primary particle in traversing ΔX to obtain a new initial energy for the subsequent increment of path. Steps 1 through 5 are repeated until the primary particle has completed its path through the detector. The entire process is then repeated for each event; i.e., each primary particle traversing the detector. The number of events chosen for a particular run is the number necessary to reduce statistical variations.

SECTION III. PROPORTIONAL COUNTER HODOSCOPE

A. Experimental Results on Secondary Electrons

A proportional counter hodoscope of the Charpak geometry [1] has been proposed [10] to measure the trajectories of cosmic rays throughout the charge spectrum. To distinguish the heavy cosmic ray tracks from the many secondary electrons, two discriminators are employed on each wire [11]. The lower discriminator is set below the minimum ionizing ($Z = 1$) distribution, and the upper one is set so that stopping electrons will seldom trigger it.

In order to observe experimentally the effects of secondary electrons produced in a MWPC, a small hodoscope was constructed by two of the authors and exposed in a 530 MeV/nucleon nitrogen beam at the Princeton Particle Accelerator. The details of the proportional counter construction will be described separately but are shown schematically in Figure 8. The detector is made of modules, each of which consists of 21 parallel anode wires spaced 0.5 cm apart, equidistant between cathodes, constructed from stainless steel wire mesh in the form of planes. These cathode planes are spaced 1 cm apart. The 0.05-mm diameter beryllium-copper anode wires are silver plated and drawn through a die to obtain a smooth surface. The photograph in Figure 9 shows these modules. The complete detector, shown in Figure 10, is constructed by combining eight modules with the anode wire planes placed alternately in perpendicular directions. A gas mixture of Ar (90%) + CO_2 (10%) was allowed to flow through the detector during operation.

The counter gain of the hodoscope was changed during the accelerator run by varying the cathode negative high voltage. A high voltage of -1900 V, which corresponds to requiring an energy deposition of approximately 2.0 keV to set the low level discriminator, gave a high percentage of events where the high level discriminator was set only along the track of the primary. Results obtained at this voltage were used to make

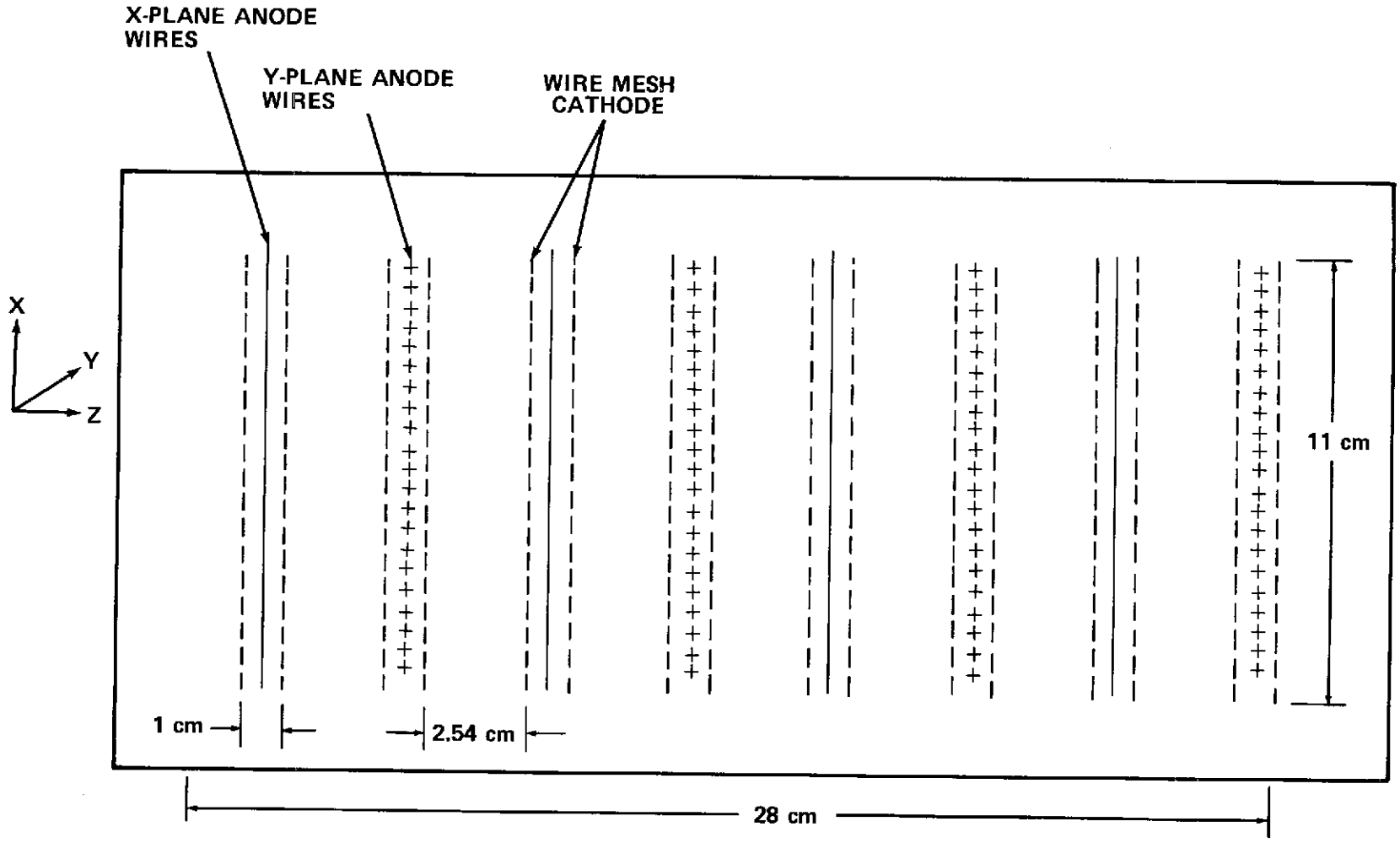

Figure 8. MWPC hodoscope configuration.

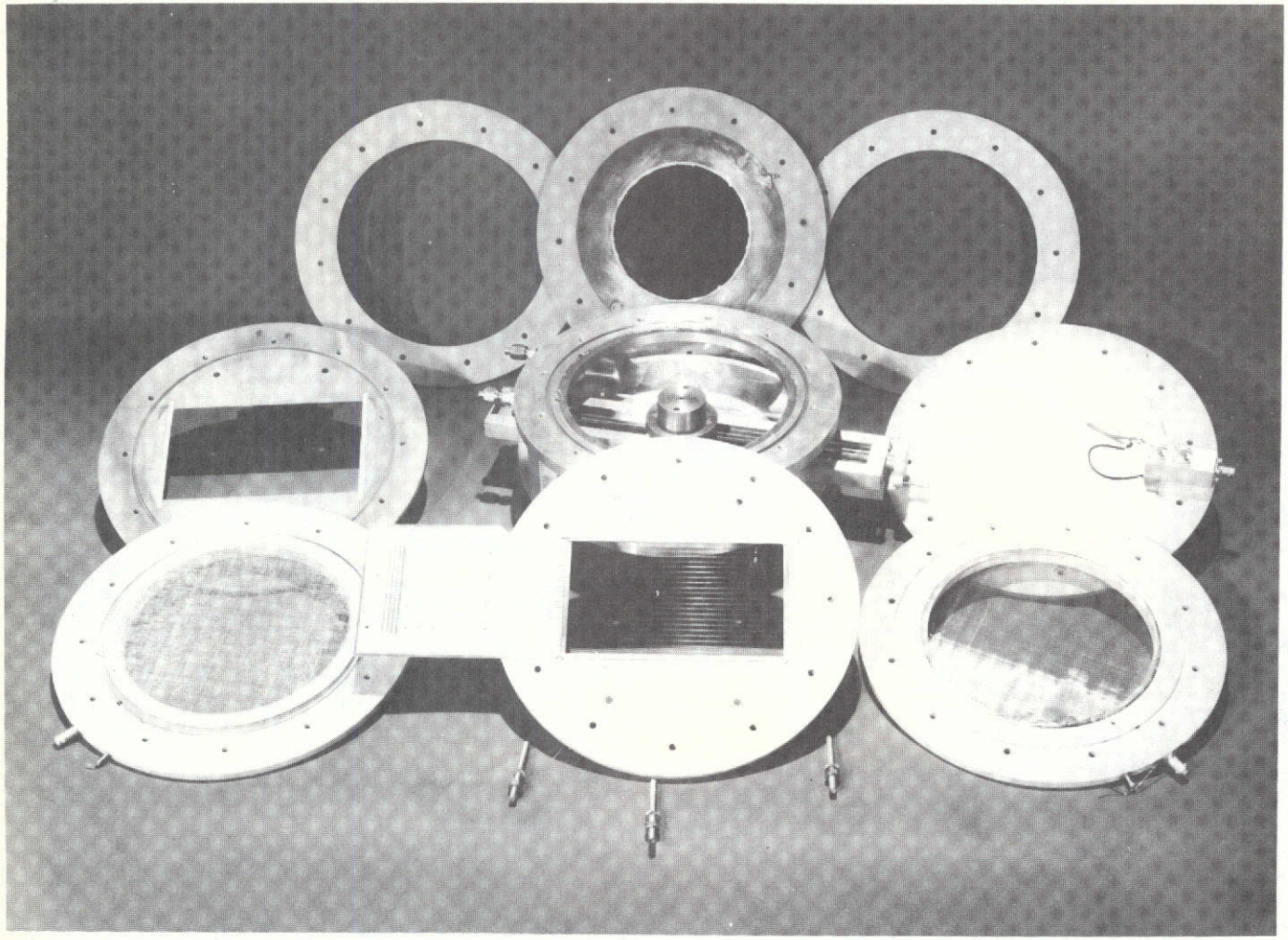

Figure 9. MWPC module used in the experiment.

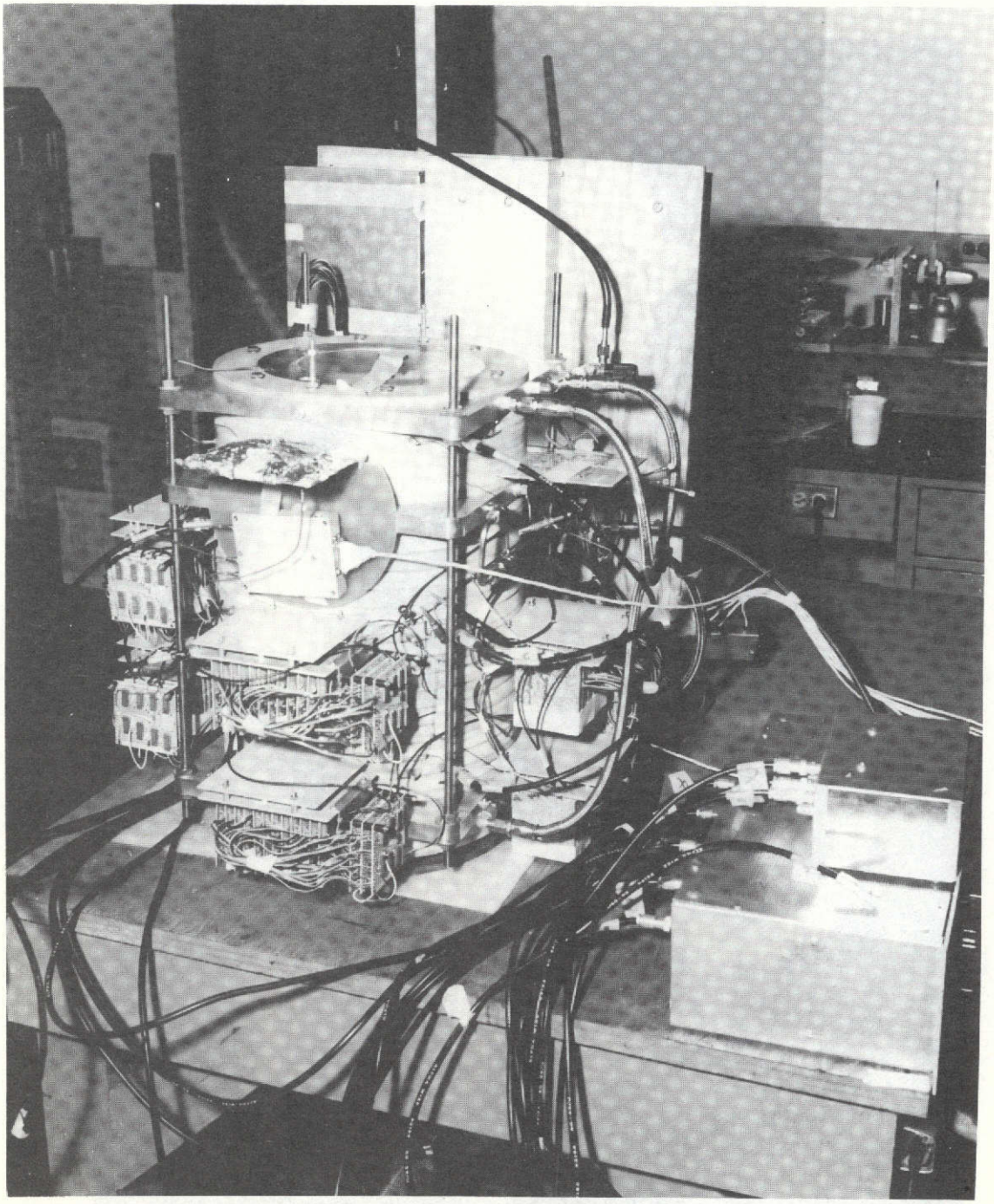

Figure 10. Complete MWPC hodoscope.

comparisons with those calculated. This report does not include a complete analysis of the results obtained from the Princeton Particle Accelerator, which will be reported separately, but a comparison is made with some of the data to determine the validity of the analysis method employed here.

B. Simulation of Discriminator Threshold Setting

The electrons produced by the heavy ion in the detector will move through the gas of the MWPC, producing other free electrons which begin to drift toward the nearest anode wire. Because of the high field near this wire, these electrons rapidly move toward the anode, leading to a multiplication of interactions with the gas and creating an avalanche of ions. It can be shown [1] that the net result is simultaneous pulses of opposite polarity on adjacent electrodes. For example, if a negative pulse builds up on the wire around which the avalanche occurs, then a positive pulse will appear on the adjacent wires. Therefore, if an amplifier is made sensitive only to the negative pulses, the volume about each wire will act as an independent counter [12]. The counter cell sensitive volume for a particular electron which creates an avalanche will, thus, have a value of approximately one-half the distance between the wires. For purposes of the calculation discussed in Section II-C, one may assume as a first approximation (Fig. 11) that any electron entering this volume would create an avalanche and, thus, "set" that particular wire. However, in the experiment the wires were set when the energy deposited in a counter cell was above the threshold level determined by the discriminator setting.

The counter cell sensitive volume may be considered in more detail by noting that the energy deposited by an electron in a given volume depends, among other parameters, upon its path length in that volume. Thus, those electrons that traverse the corner of a counter cell will deposit less energy than those passing nearer the anode wire. Therefore, one is able to crudely simulate different levels of energy deposition and, thus, discriminator settings by varying the sensitive volume of a counter cell. To determine the sensitivity of the volume parameter, the authors made computer runs with 75 events, each using the following sensitive volumes (Fig. 11), and compared the probability distributions of number of wires set by off-axis electrons:

1. 1.0 cm by 0.5 cm by 11.0 cm (GEOMETRIC VOLUME)
2. 0.5 cm by 0.5 cm by 11.0 cm
3. 0.3 cm by 0.5 cm by 11.0 cm

These results are shown in Figure 12 along with the results from the experiment. One notes that the third case is in close agreement with the experiment. The figure also shows that the difference between the calculated point and the experiment is greatest for wire 1. This can be explained by noting that most of the electrons that set the nearest wire

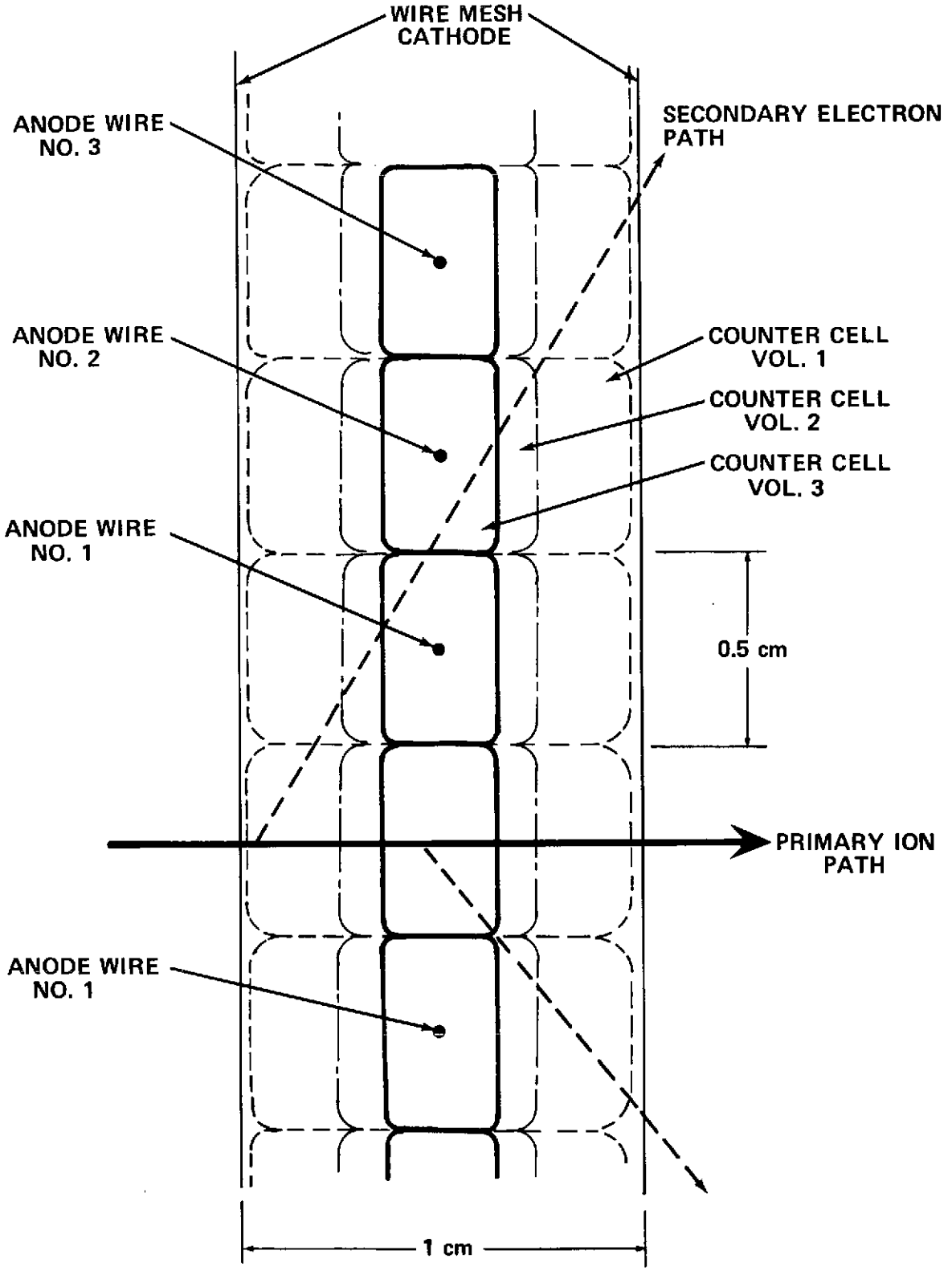

Figure 11. Cross sectional view of counter cell with sensitive volumes indicated.

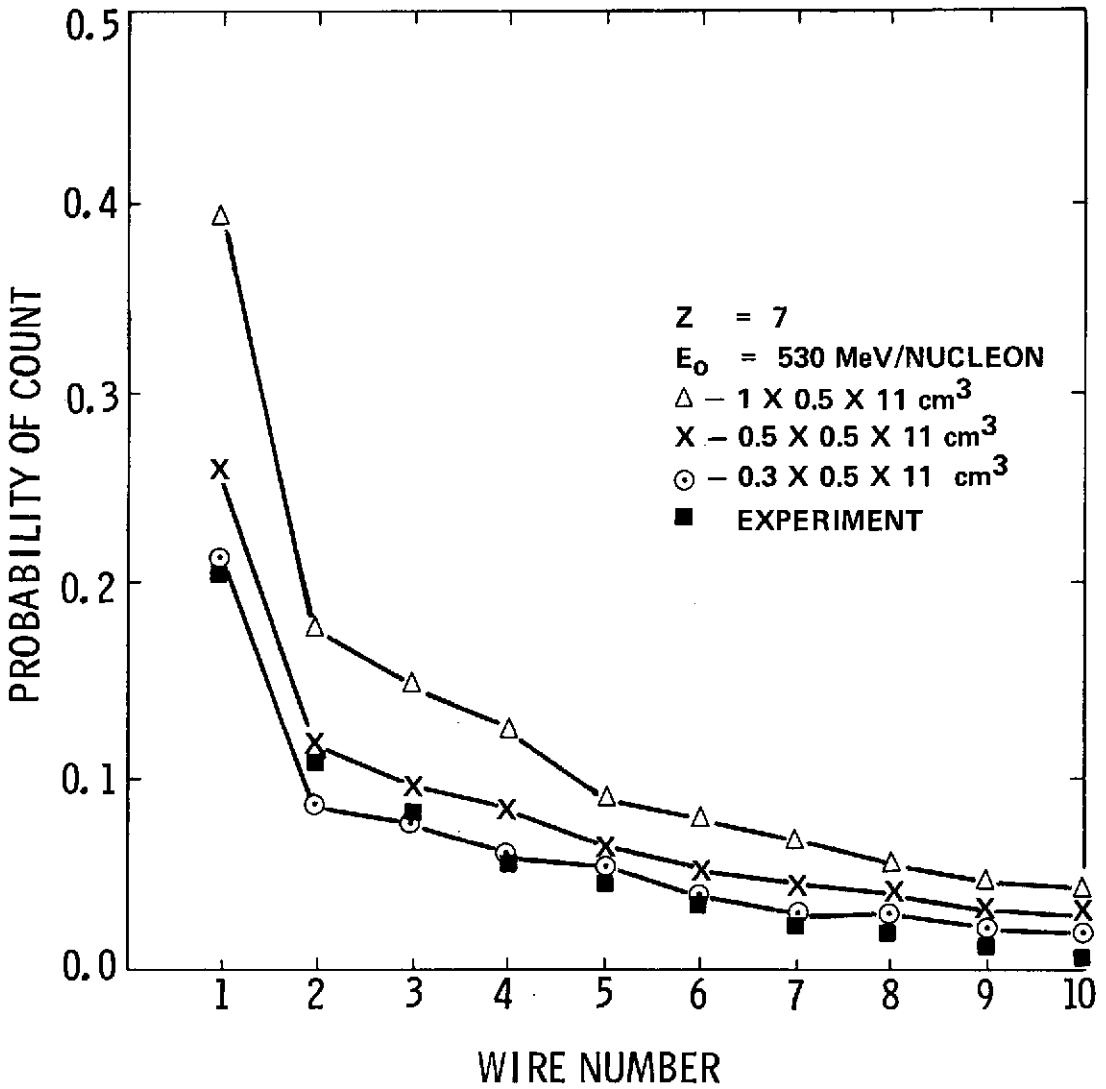

Figure 12. Variation of probability of setting off-axis wires with counter cell sensitive volume.

have low energies. High-energy electrons are primarily scattered in the forward directions, while the lower energy ones are not. Thus, low-energy electrons are more likely to be scattered away from their initial direction and may not reach the counter cell. This is less likely to be the case for the high-energy electrons which primarily set the wires further away from the primary particle's track. Therefore, since the simplified calculation neglects multiple scattering of electrons, this method will tend to overestimate the probability of setting wire 1.

SECTION IV. RESULTS

A. MWPC Hodoscope Results

The computer code described in Section II-C has as part of its output an option for a graphic display of the simulation from an SC4020 plotter. This display shows the configuration of the particular hodoscope used in the simulation, including the electrodes, the projection of the electron paths in the X-Z and Y-Z planes, and the anode wires that are set during the event shown. An example is shown in Figure 13 for the X-Z plane and in Figure 14 for the Y-Z plane of an event depicting a 530 MeV/nucleon nitrogen nucleus traversing the hodoscope described in Section III. The dotted lines in the figures indicate the cathode mesh planes, the vertical lines depict the anode wires in the plane being shown, and the (+) symbol indicates the anode wires in a plane perpendicular to this plane. The primary particle is assumed to travel along the axis of the detector, the Z axis. The dashed lines show the projection of the electron's path. The L's at a particular wire location indicate that in the simulation an electron entered the sensitive volume of that counter cell.

Figure 15 is an illustration of a typical event from the separate computer analysis of the experiment. The L's indicate that the low-level discriminator was triggered for that particular wire, while the B's indicate that both the high- and low-level discriminators were set. One notes from the figure that the primary particle's path is clearly distinguishable by the line passing through the B's and that the pattern of the L's is similar to that obtained from the simulation shown in Figures 13 and 14.

Figure 16 is a plot of the probability of a particular wire being set by an off-axis electron. The calculated results are from 2000 events and the experimental points using 200 events. The counter cell sensitive volume used for the calculation was 0.3 cm by 0.5 cm by 11 cm. The agreement between the experiment and calculated value is quite close.

Figure 17 shows a comparison between the experiment and simulation for the frequency distribution of the number of wires set based upon the same events as were used in Figure 16. Again, one notes that there is close agreement.

B. A More Complete Modeling

A second, more complete Monte Carlo modeling of the electron energy transport process was constructed [13]. This model differs from the simple one in the following ways: the Moliere multiple scattering distribution was used to describe the movement of electrons through the medium rather than the "straight-ahead" approximation, the energy deposited by electrons was calculated using the electron mean stopping power, the

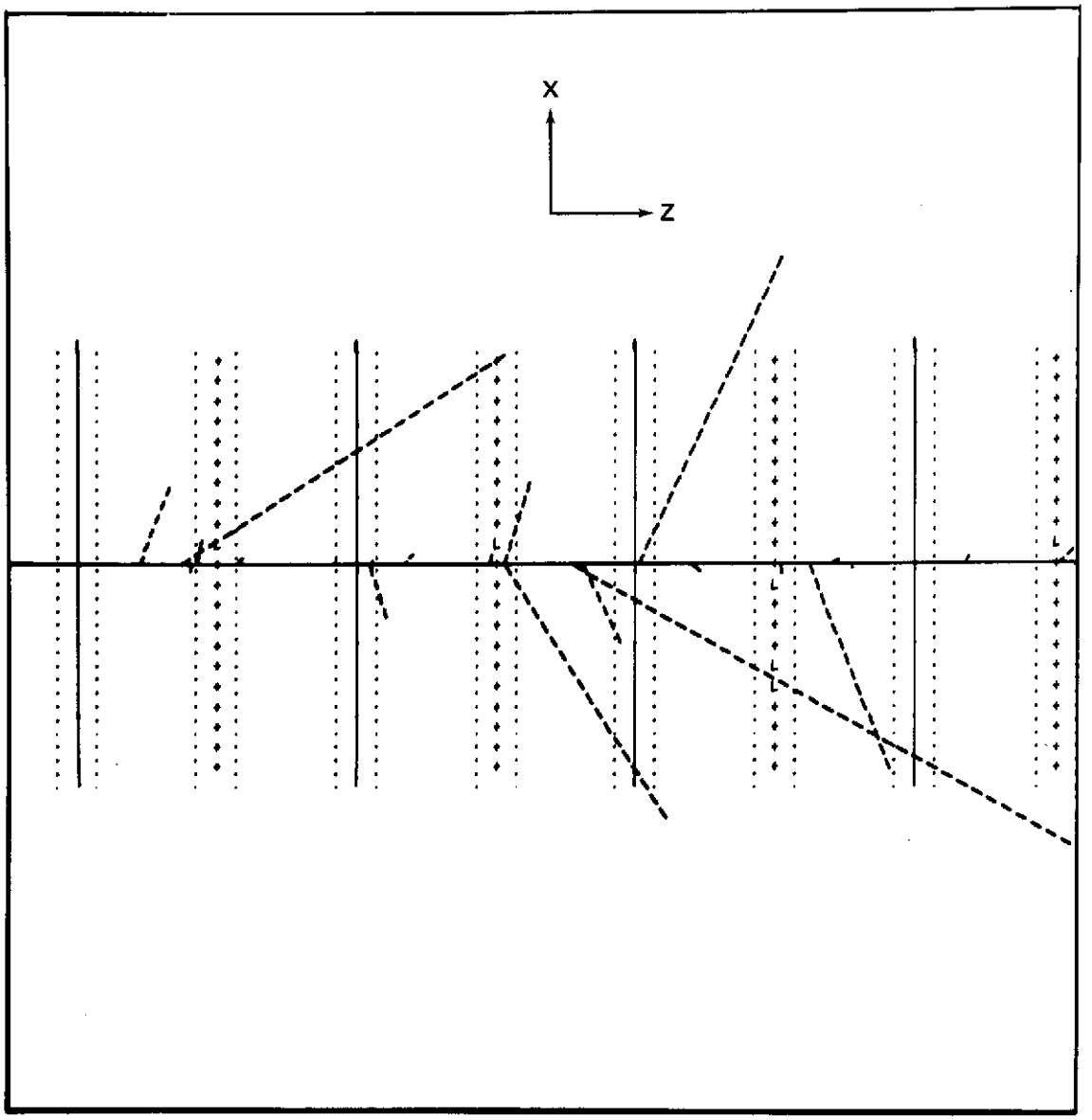

Figure 13. Graphic display of simulation of 530 MeV/nucleon nitrogen nuclei in a MWPC hodoscope, X-Y plane.

detector geometry could be more completely described including the production and transport of electrons in the detector walls, and the frequency distribution of energy deposition in a rectangular box about each wire was tabulated rather than assuming that

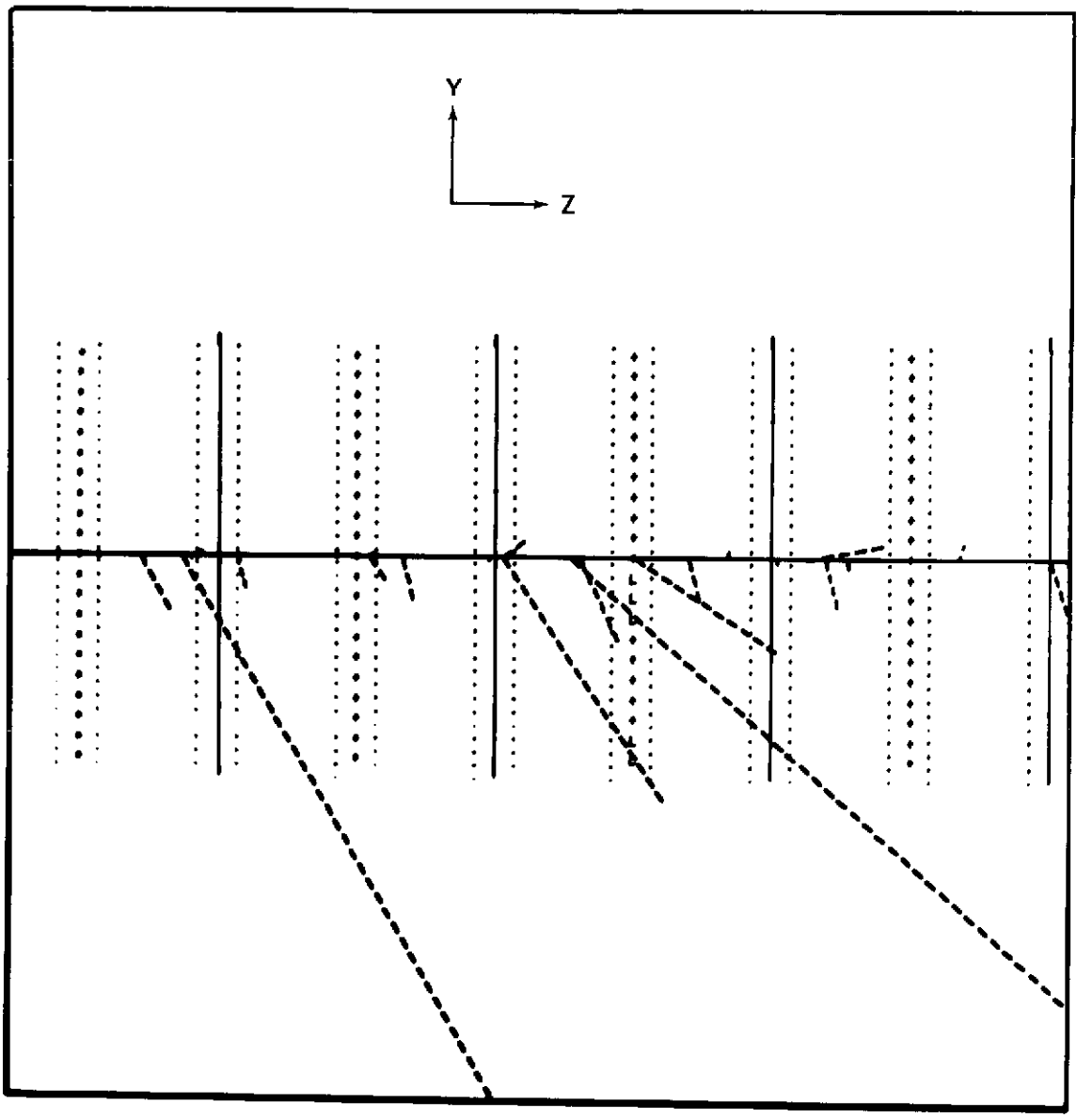

Figure 14. Graphic display of simulation of 530 MeV/nucleon nitrogen nuclei in a MWPC hodoscope, Y-Z plane.

the wire was set by any electron entering the box. Figure 18 shows a comparison of the results of this model with experiment and with the simple model for nitrogen nuclei at 530 MeV/nucleon. A front wall of 0.254-cm-thick aluminum was included in the more complete model, and electrons which deposited more than 2 keV around a wire were

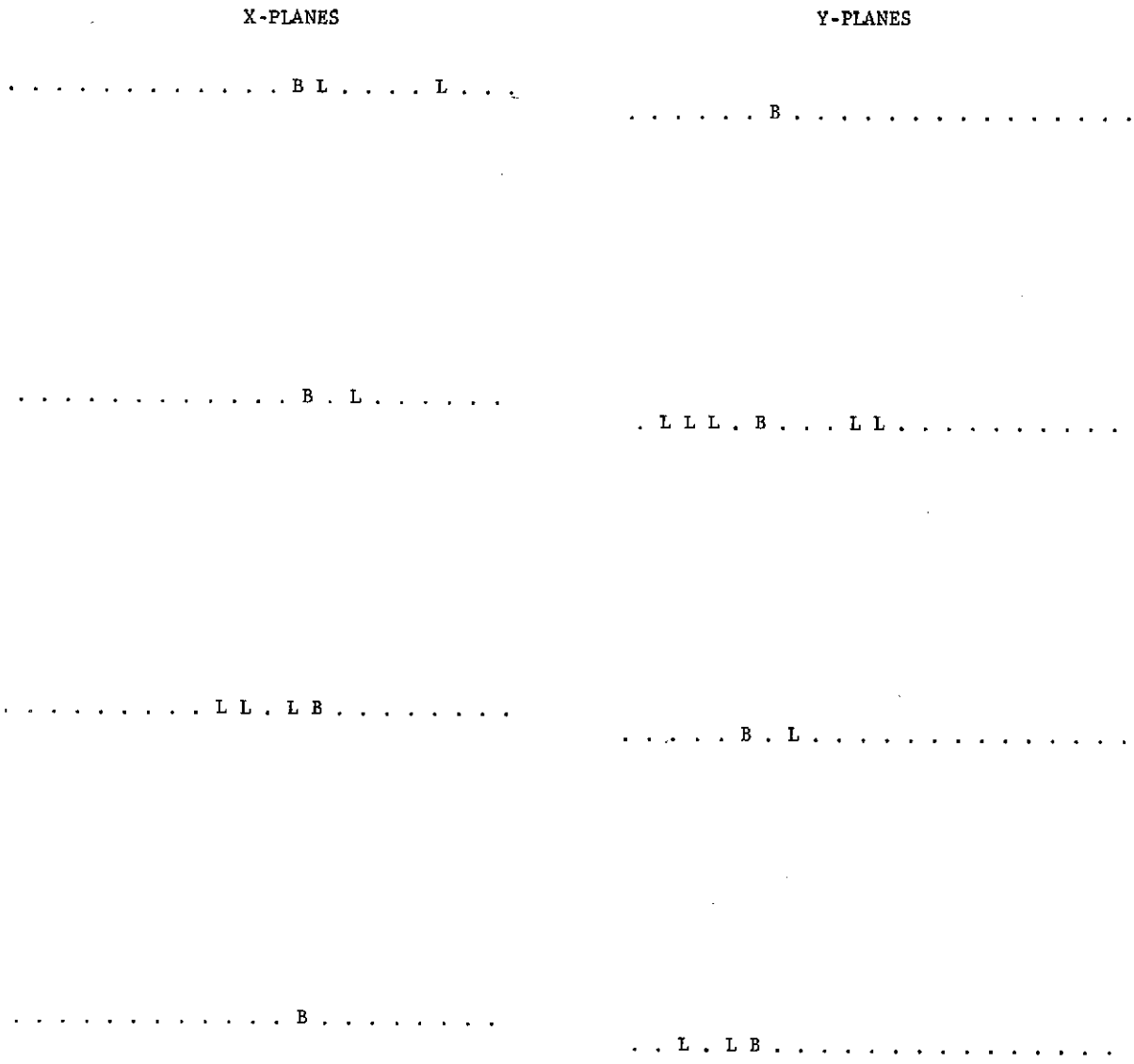

Figure 15. Sample results from experiment using 530 MeV/nucleon nitrogen nuclei in accelerator beam, HV = -1900V.

assumed to set it. The box surrounding each wire was 0.5 cm by 1 cm by 50 cm. From the figure, it appears probably that about 2 keV at a cathode high voltage setting of -1900 V was required to set a wire in the experiment. (The complete frequency distributions of energy deposition about each wire are shown in the Appendix.)

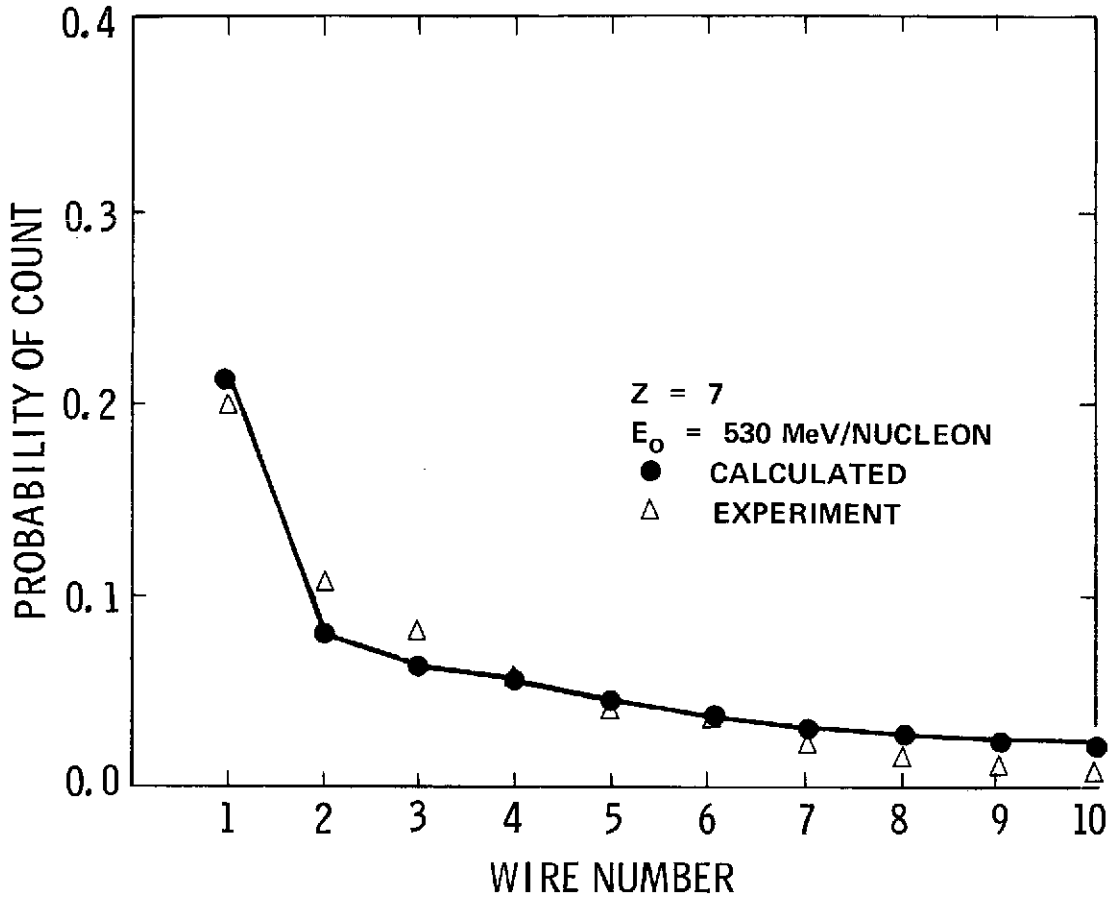

Figure 16. Probability of setting off-axis wires (comparison of calculation and experiment).

C. Predictions for High-Z Particles

The previously described method may be used to make estimates of electron background produced in a hodoscope by high-Z relativistic particles. Figure 19 shows the probability distribution of off-axis wires set for the 530 MeV/nucleon ($\beta = 0.769$) nitrogen case previously discussed and 10 GeV/nucleon ($\beta = 0.996$) iron ($Z = 26$) and silicon ($Z = 14$) nuclei. The sensitive volume of the counter cell was assumed to be the same as that used in Figure 16. The indication from the figure is that, for example, one would expect the wires closest to the iron track to be set in almost four out of five events, and the second wires for about one-half the events. Since a 2 GeV/nucleon ($\beta = 0.95$) oxygen nucleus loses approximately the same energy in the hodoscope as the 530 MeV/nucleon nitrogen nucleus, this case is shown to illustrate that the probability

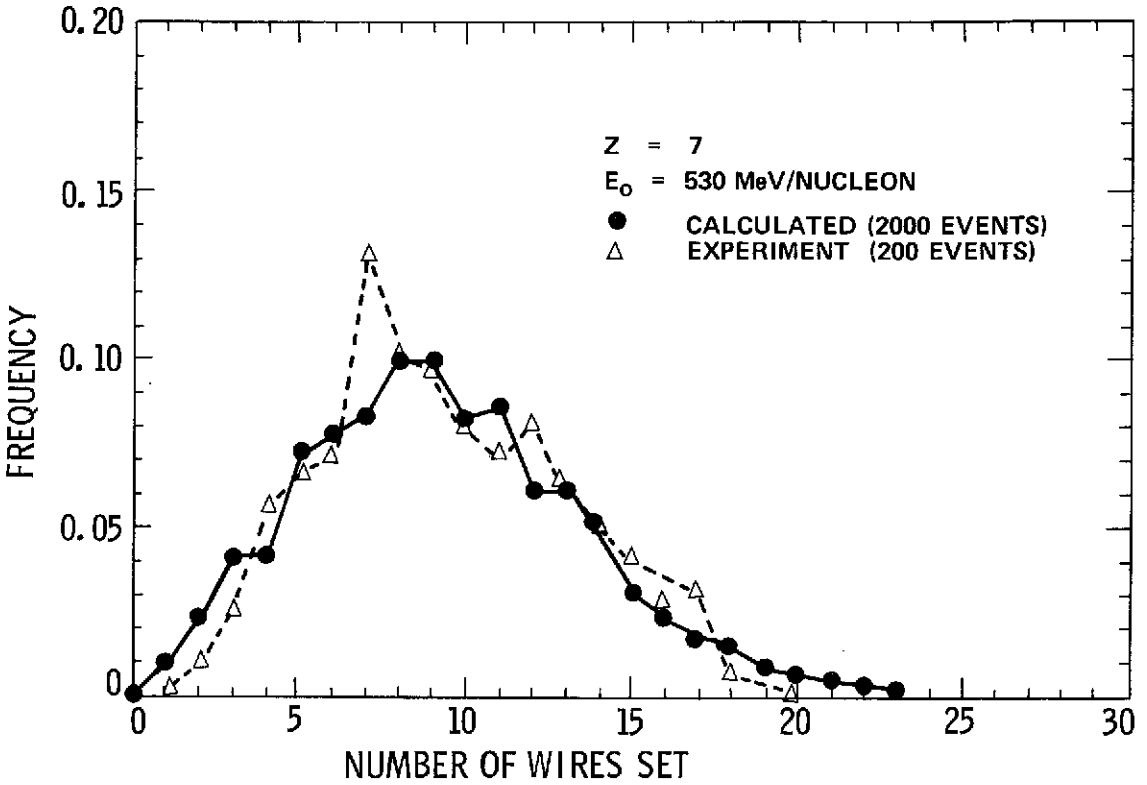

Figure 17. Frequency distribution of off-axis wires set.

distribution is essentially the same but with a slight rise for wires further from the primary track because of a higher E_m for the faster oxygen nucleus.

Figures 20 and 21 show the SC4020 graphic display from the computer simulation for a typical 10 GeV/nucleon iron event. When one compares these figures with Figures 13 and 14 for nitrogen, one notes the dramatic effect that the Z^2 dependence makes in electron production in the hodoscope.

Figure 22 shows the results from the simplified Monte Carlo calculation of the frequency distribution for the number of wires set for Z = 7, 14, and 26, all having initial kinetic energy of 10 GeV/nucleon. One sees from the figure that as the primary particle charge increases, the distribution becomes broader and more symmetrical and that individual charges probably could not be resolved using these distributions alone since there is significant overlapping. This distribution obviously depends upon the dimensions and number of wires that a particular MWPC hodoscope has. This is especially true for the higher-Z primary particles. The trend toward symmetry of this distribution as Z

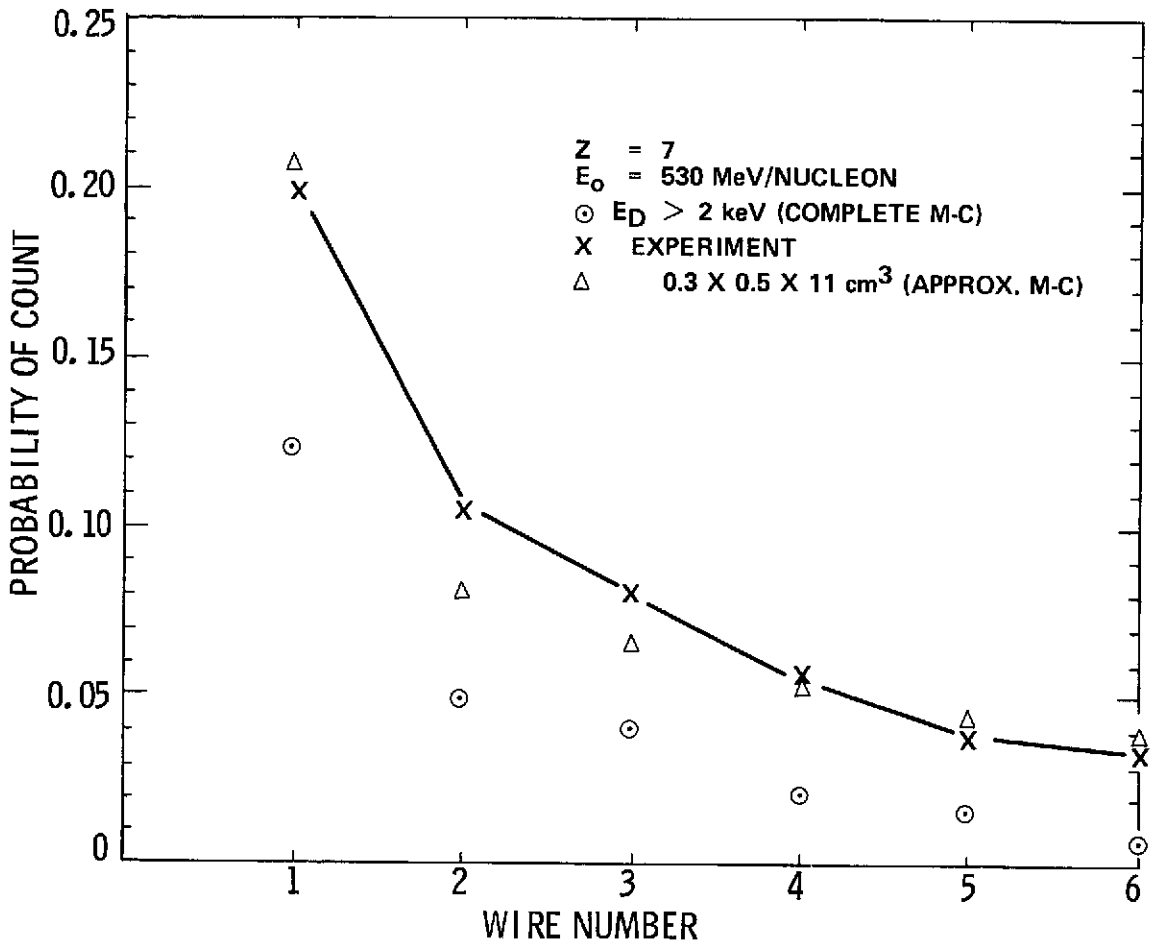

Figure 18. Probability of setting off-axis wires (comparison of two methods of calculation and experiment).

increases is, of course, a consequence of assuming a Poisson distribution for the number of delta rays produced by the primary particle. Since the Poisson distribution approaches the Gaussian distribution for sufficiently large values of ⟨N⟩ and since ⟨N⟩ is proportional to Z^2, then one would expect the frequency distribution of number of wires set to follow this trend.

Figure 23 shows the Vavilov distribution of energy loss by a 10 GeV/nucleon iron nucleus in 28 cm of argon at 1 atmosphere. One notes by comparing this figure with Figure 1 that the iron distribution is more symmetrical. One also notes that the distribution shown in Figure 23, like those in Figure 22, becomes broader as Z increases.

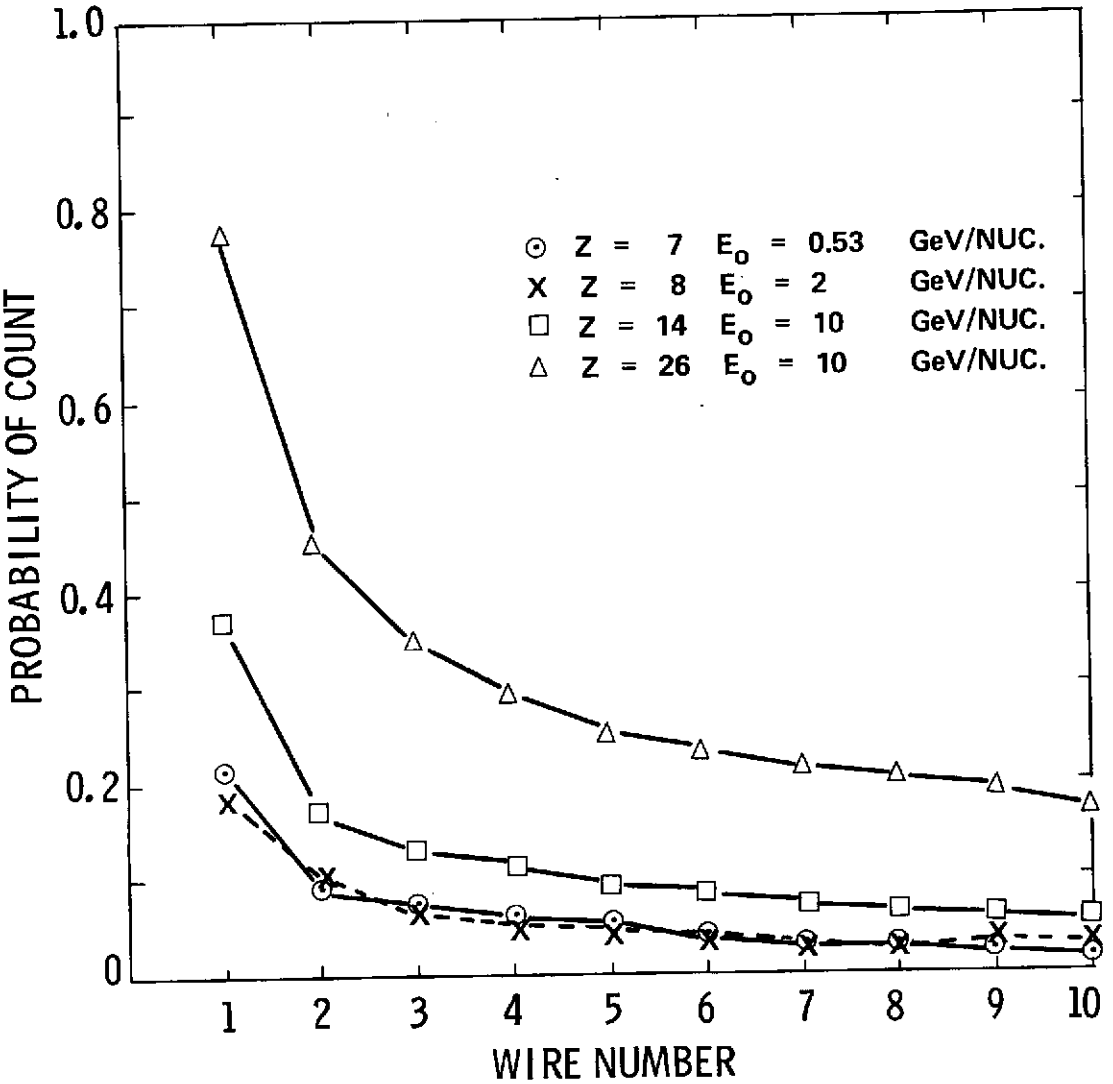

Figure 19. Probability of setting off-axis wires for different nuclei.

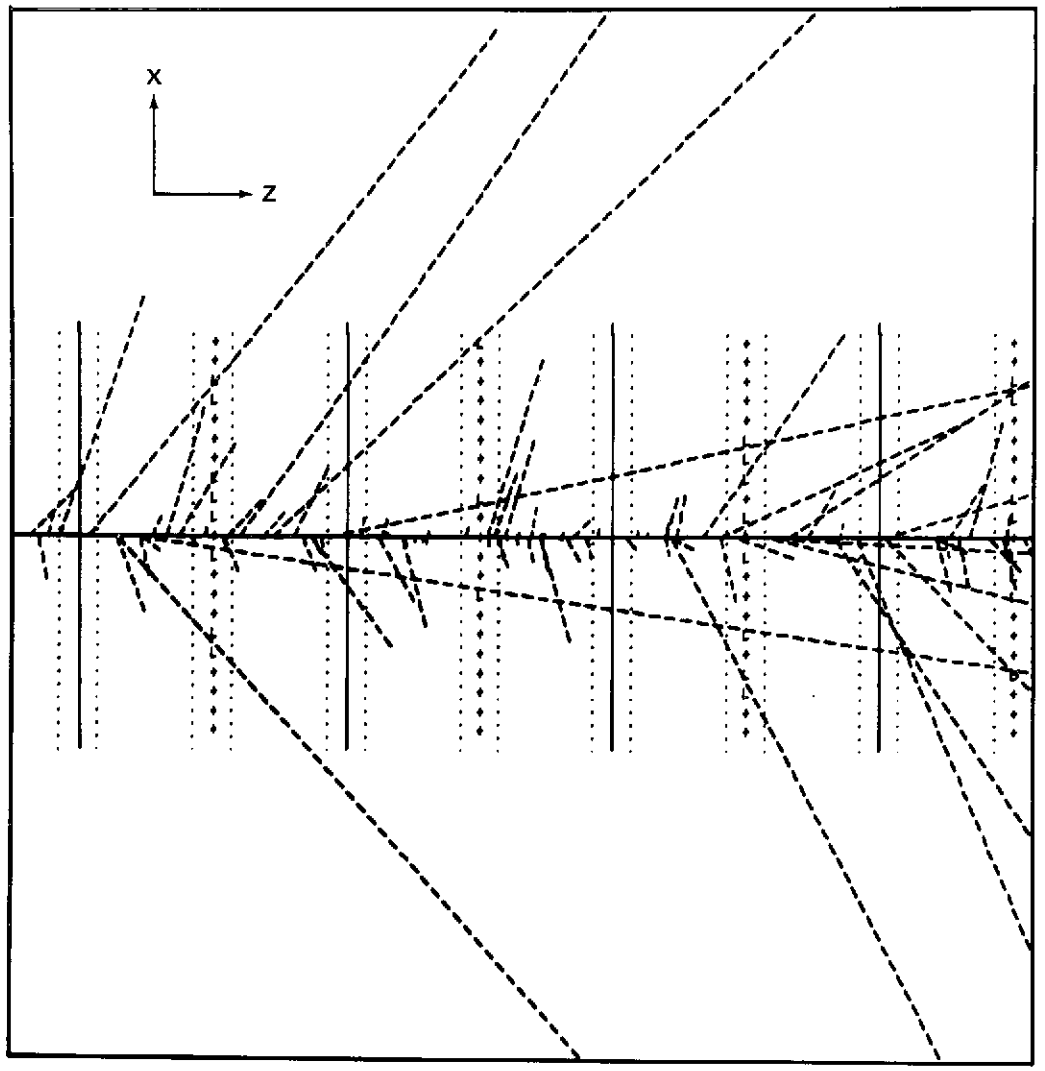

Figure 20. Graphic display of simulation of 10 GeV/nucleon iron nuclei in MWPC hodoscope, X-Z plane.

In fact, for high-Z relativistic primary particles traversing thin detectors, the width of the distribution is proportional to Z [14] and the Vavilov distribution approaches a Gaussian distribution [7].

SECTION V. CONCLUSIONS

The preceding results have shown that one is able to quickly estimate an upper level of the secondary electron background produced by heavy nuclei in a MWPC hodoscope using a simplified Monte Carlo model. This is possible in part because the

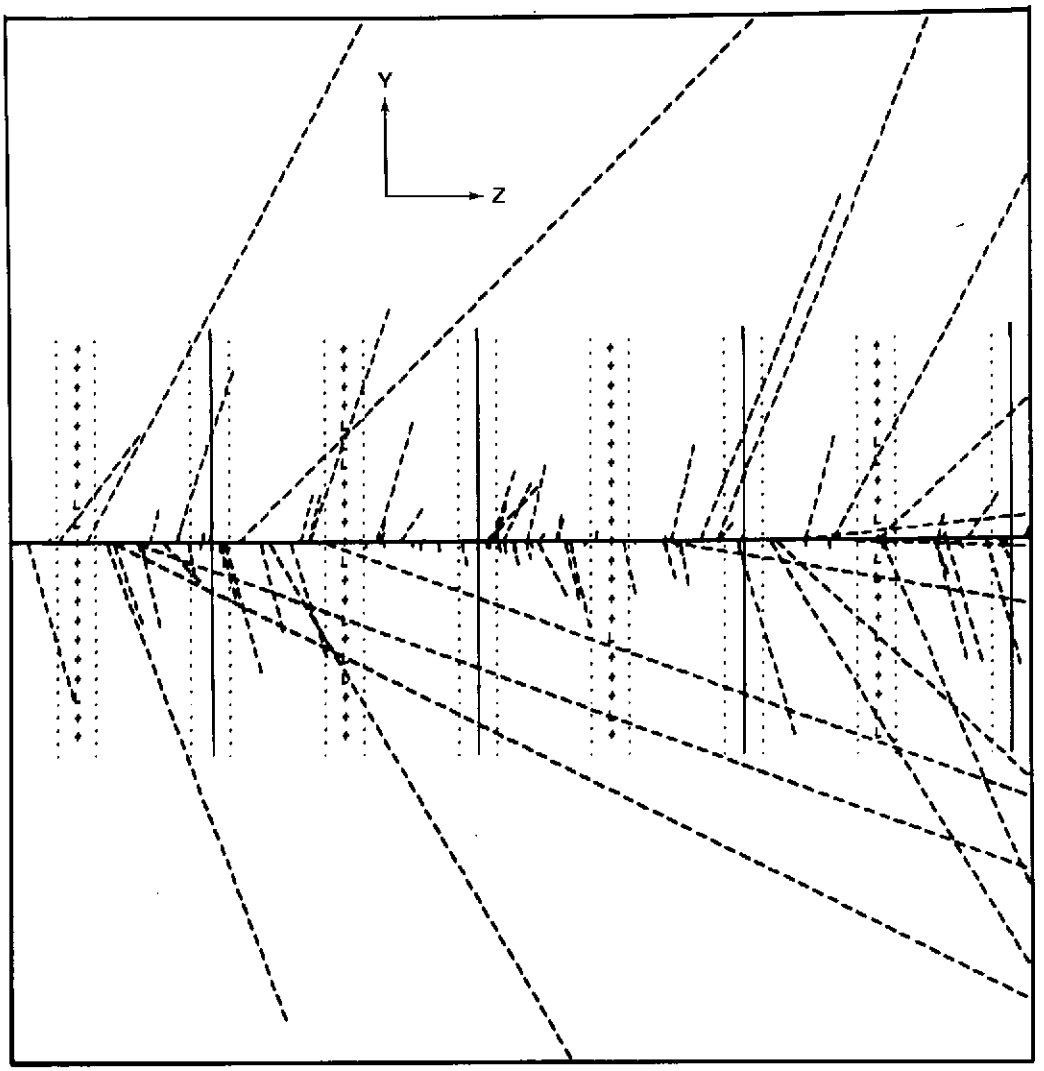

Figure 21. Graphic display of simulation of 10 GeV/nucleon iron nuclei in MWPC hodoscope, Y-Z plane.

higher energy electrons are not significantly scattered by the detector gas. Different discriminator energy level thresholds may be crudely simulated by adjusting the sensitive volume of the hodoscope counter cell. However, if one wishes to make accurate predictions based on energy deposition in counter cells, a more complete Monte Carlo method is required. This would be necessary if, for example, one wished to determine the high- and low-level discriminator threshold settings to cover a given charge spectrum of cosmic rays.

George C. Marshall Space Flight Center
National Aeronautics and Space Administration
Marshall Space Flight Center, Alabama, October 9, 1973

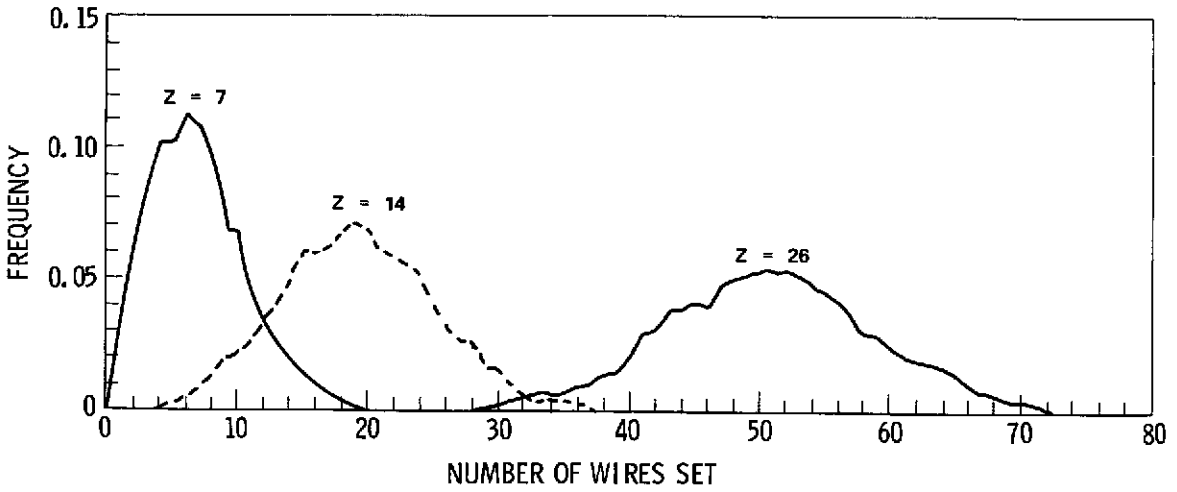

Figure 22. Frequency distribution of off-axis wires set (comparison of different nuclei).

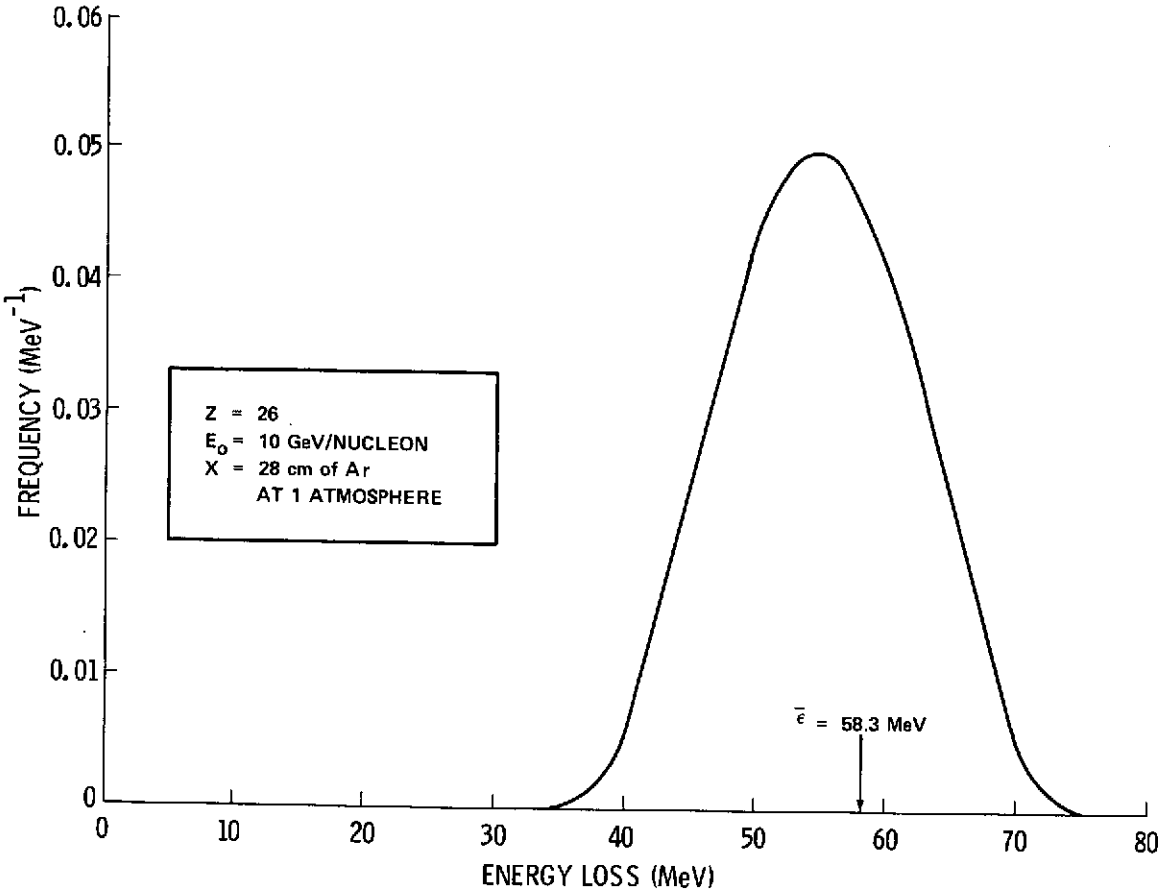

Figure 23. Vavilov distribution for 10 GeV/nucleon iron nuclei traversing 28 cm of argon at 1.0 atmosphere.

APPENDIX

ENERGY DEPOSITION BY SECONDARY ELECTRONS

Calculations of energy deposition by secondary electrons in a MWPC hodoscope using the more complete Monte Carlo model described in Section IV-B are presented in this appendix. The calculations are based on a MWPC having a 0.254-cm aluminum front wall. The counter gas is Ar (90%) + CO_2 (10%) at 1 atmosphere. Each counter cell was assumed to have dimensions 0.5 cm by 1.0 cm by 50.0 cm. The calculations were made for 10 GeV/nucleon iron and 0.53 GeV/nucleon nitrogen nuclei.

Figures A-1 through A-6 show frequency distributions of energy deposited in the counter cells around wires 1 through 6, respectively. Figure A-7 shows the probability distribution of wires set by secondary electrons from nitrogen primaries assuming two different lower levels of energy deposition required to set a wire, 0 and 2 keV. Figure A-8 is similar to Figure A-7 except that the primary ions are iron nuclei and the energy deposition levels are 0, 2, and 4 keV.

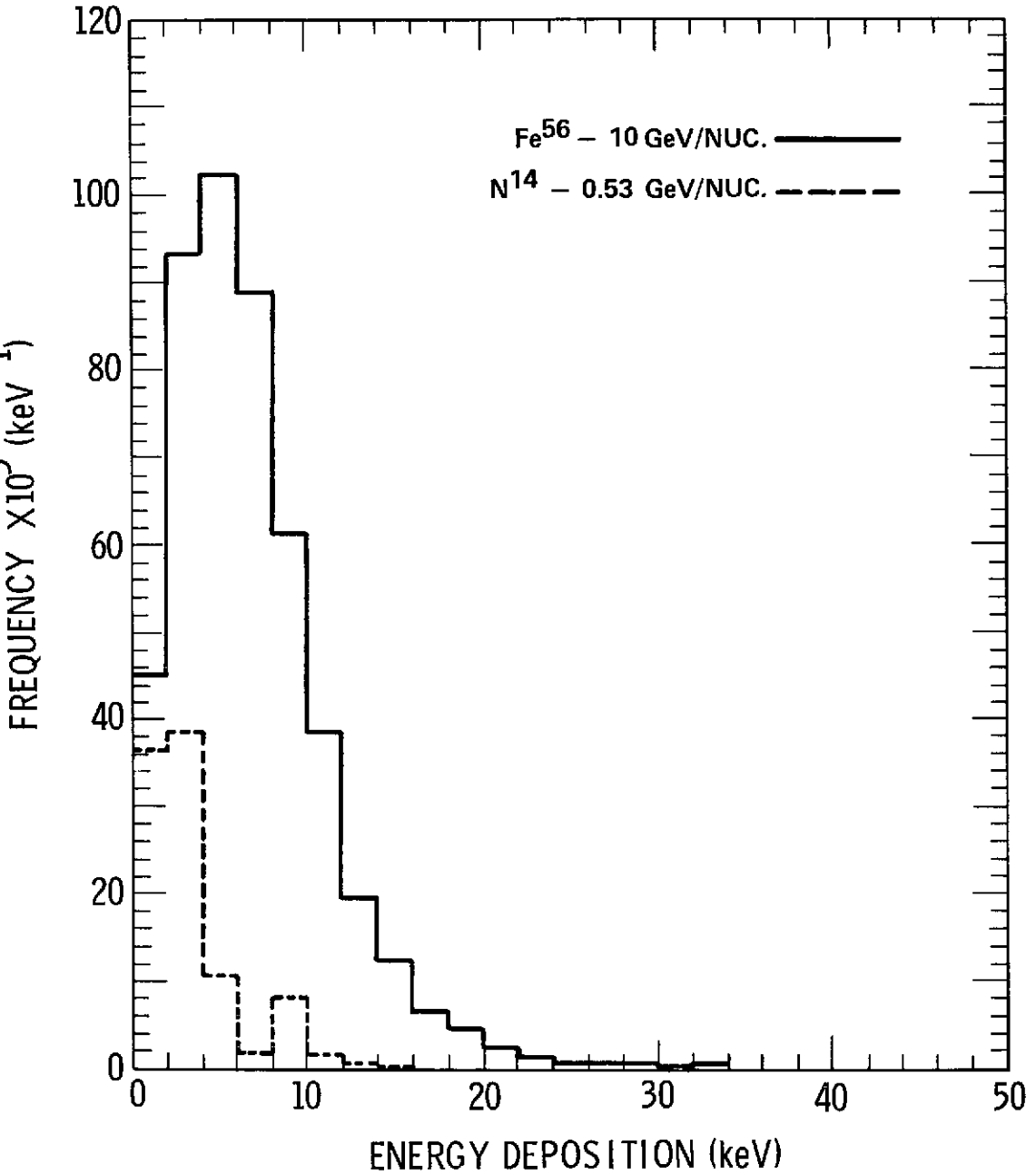

Figure A-1. Energy deposition distribution by electrons produced by 0.53 GeV/nucleon nitrogen and 10 GeV/nucleon iron nuclei in counter cell 1.0 cm from track (wire 1).

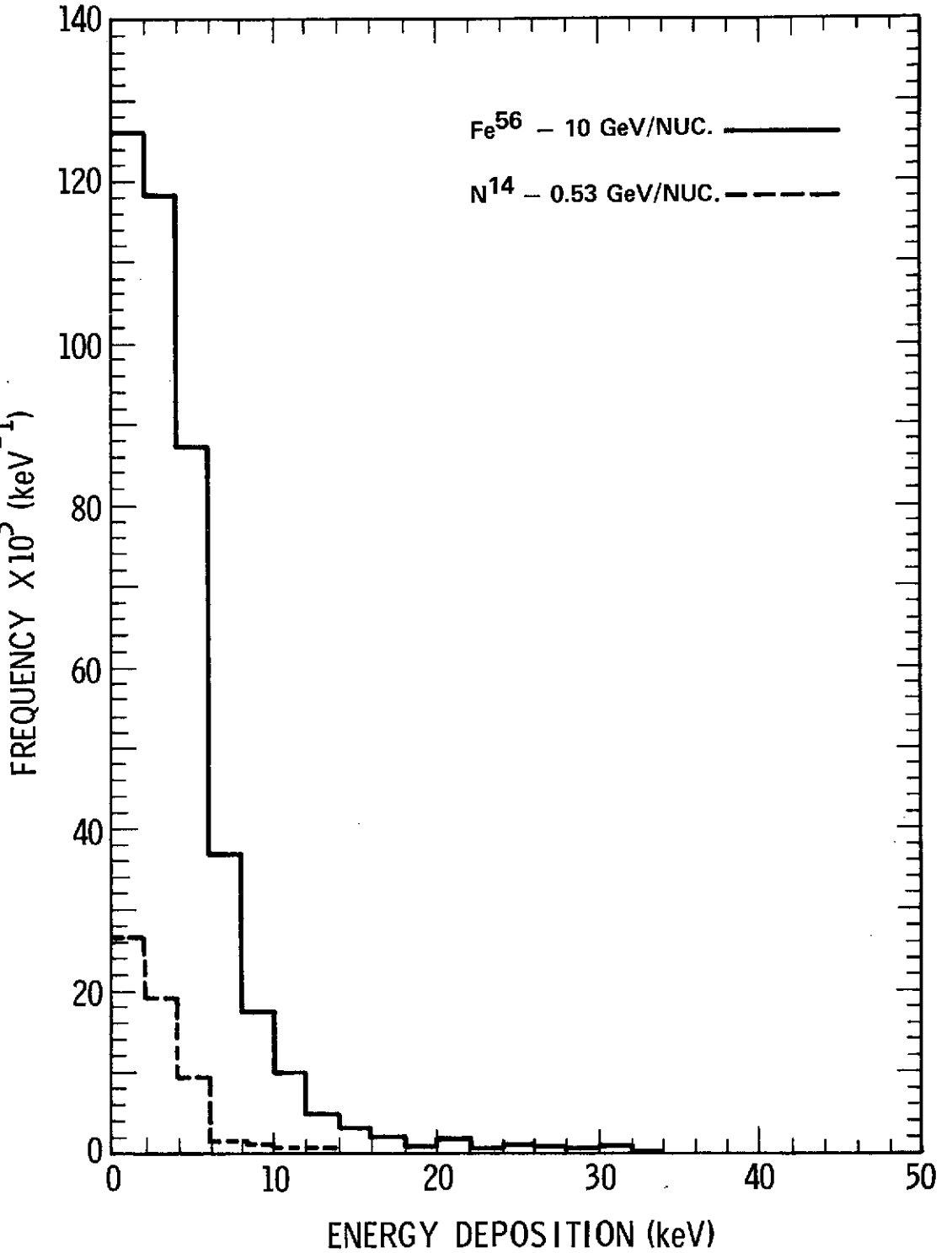

Figure A-2. Energy Deposition distribution by electrons produced by 0.53 GeV/nucleon nitrogen and 10 GeV/nucleon iron nuclei in counter cell 1.5 cm from track (wire 2).

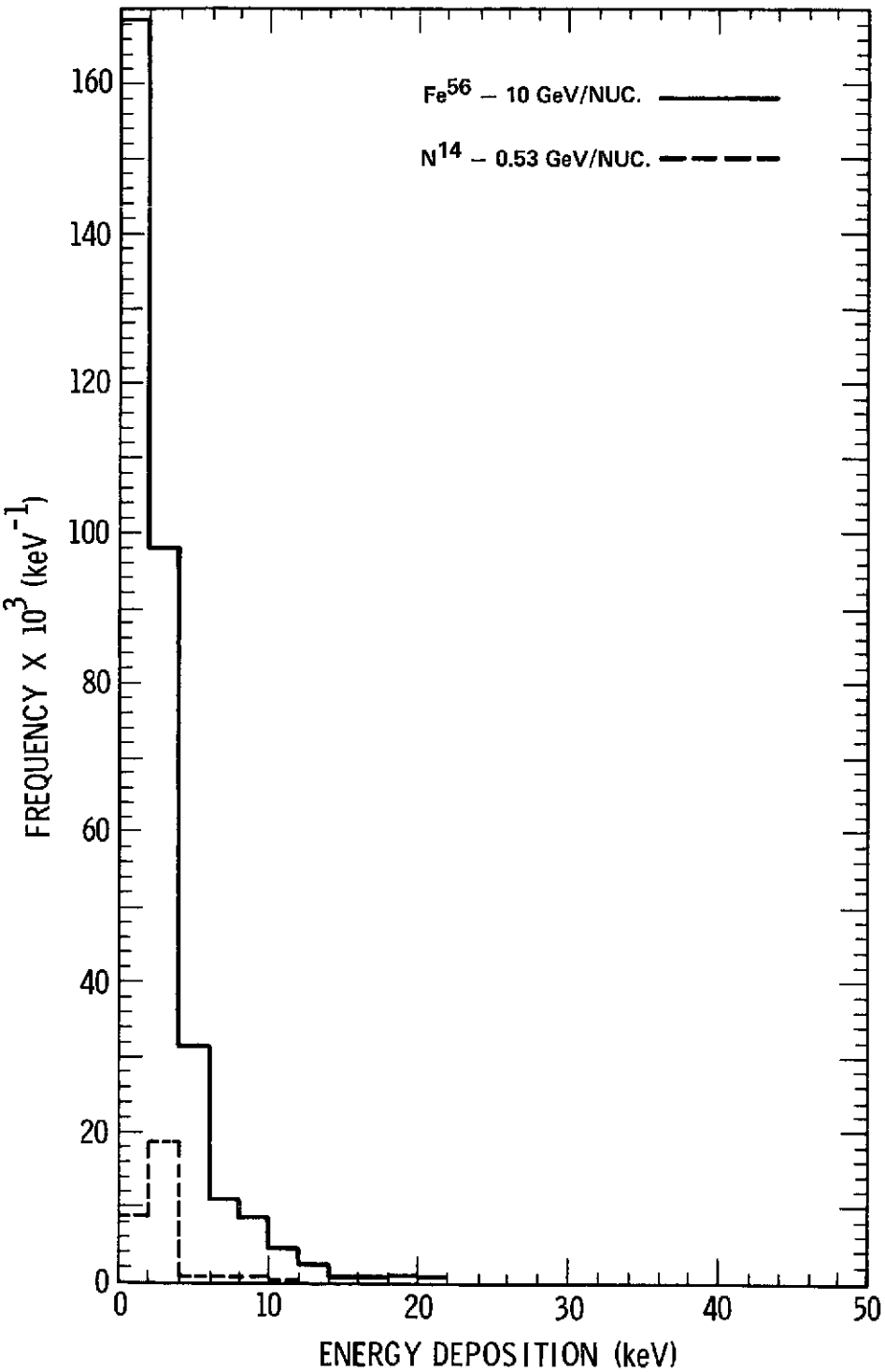

Figure A-3. Energy deposition distribution by electrons produced by 0.53 GeV/nucleon nitrogen and 10 GeV/nucleon iron nuclei in counter cell 2.0 cm from track (wire 3).

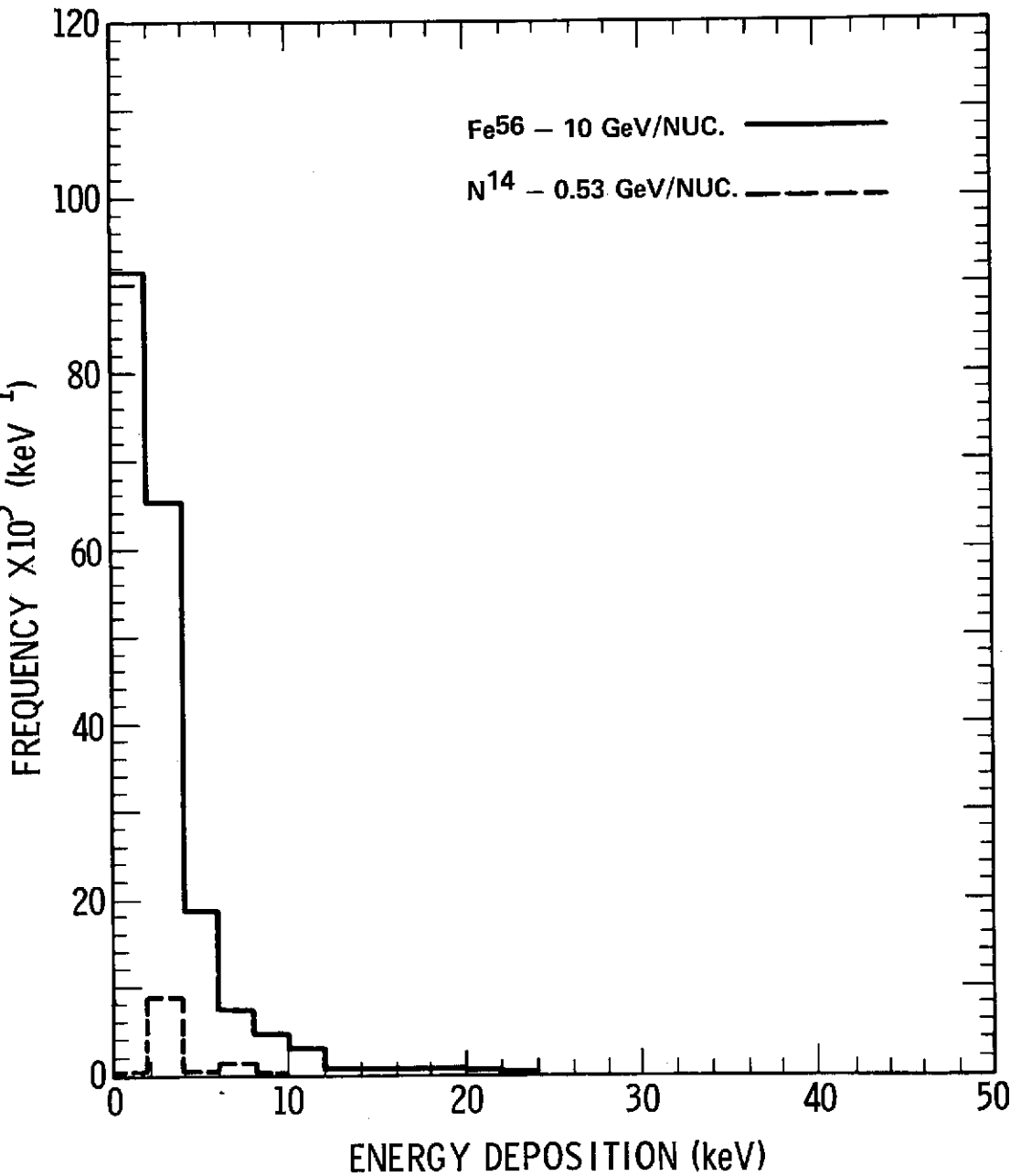

Figure A-4. Energy deposition distribution by electrons produced by 0.53 GeV/nucleon nitrogen and 10 GeV/nucleon iron nuclei in counter cell 2.5 cm from track (wire 4).

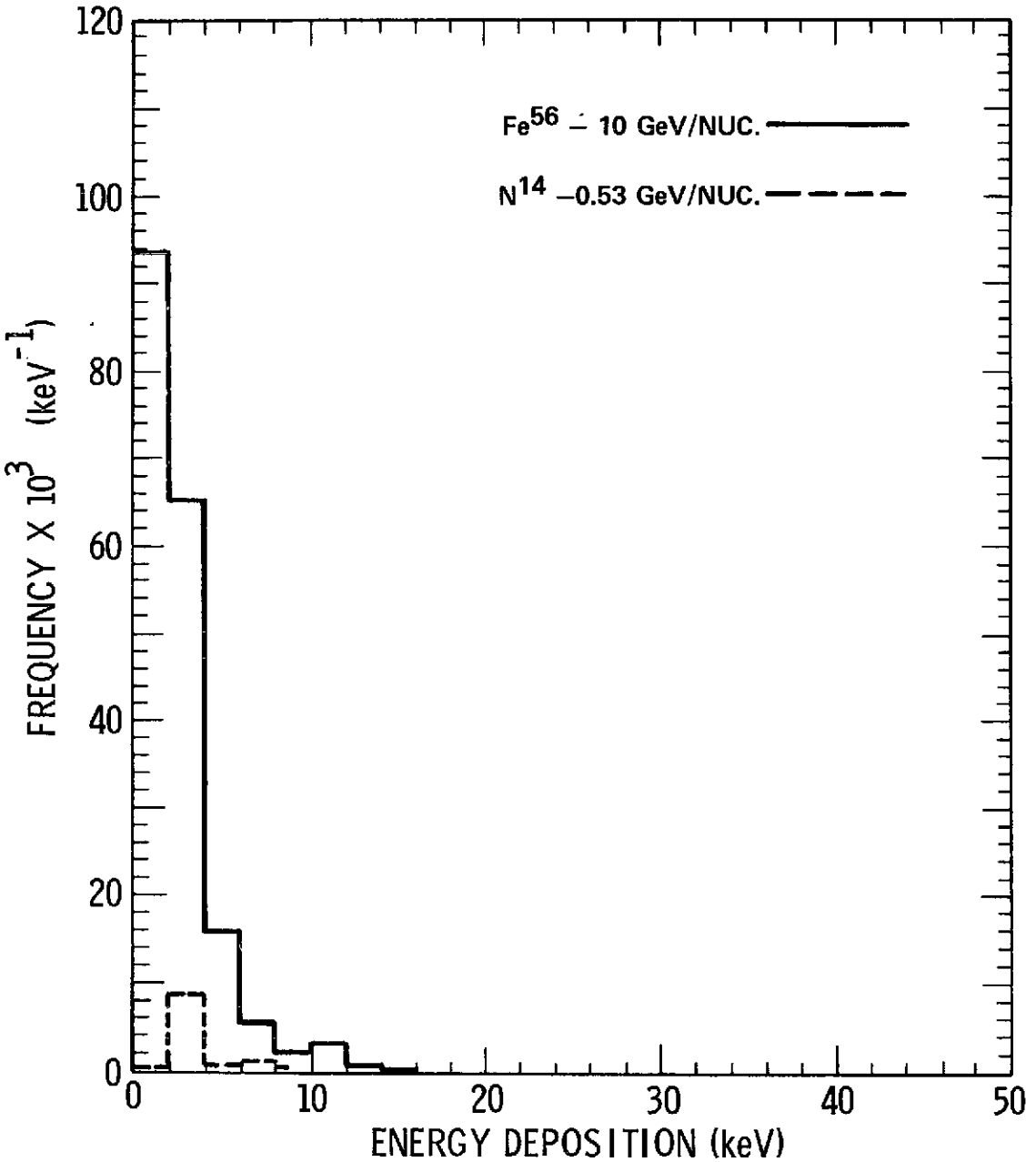

Figure A-5. Energy deposition distribution by electrons produced by 0.53 GeV/nucleon nitrogen and 10 GeV/nucleon iron nuclei in counter cell 3.0 cm from track (wire 5).

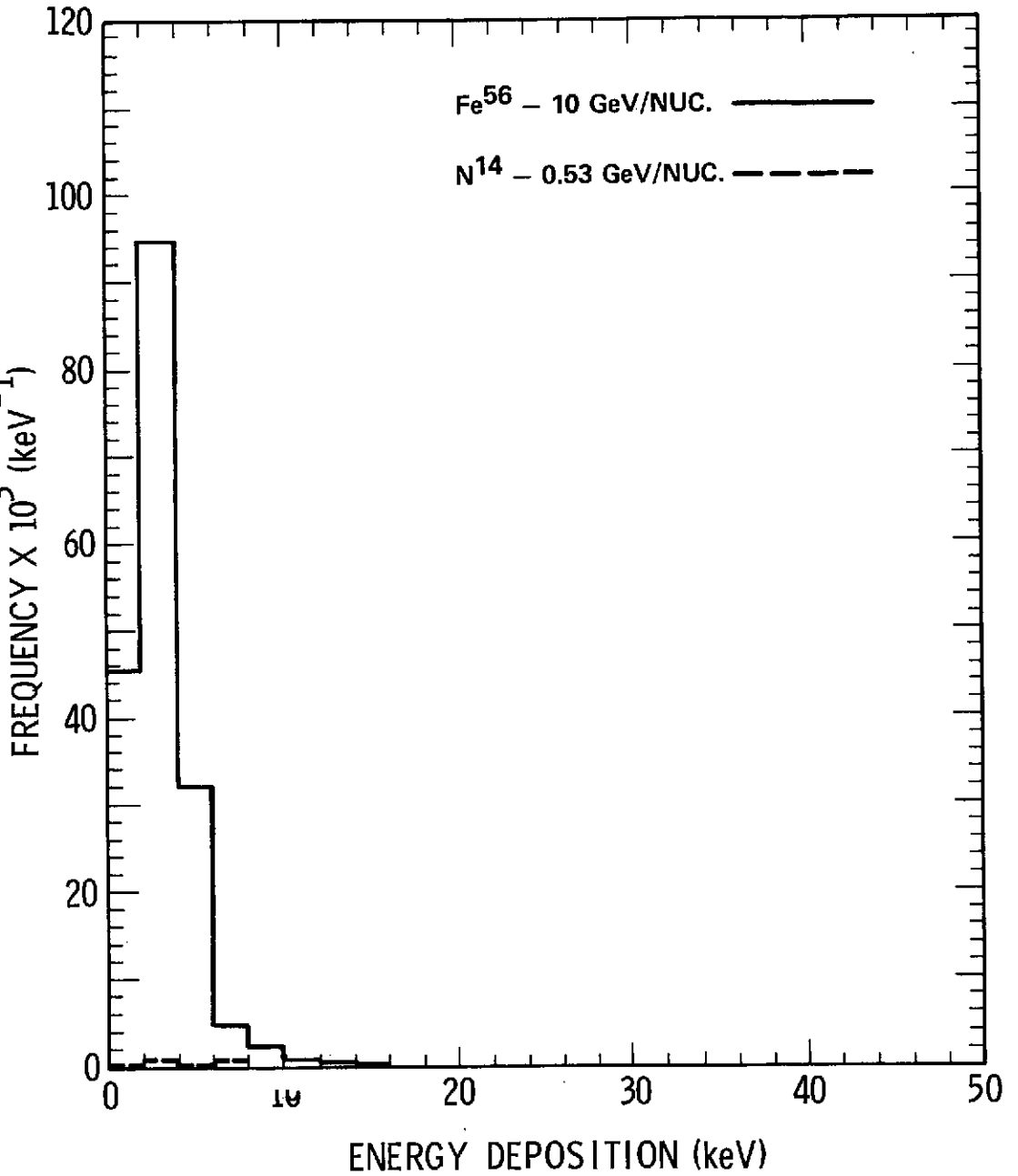

Figure A-6. Energy deposition distribution by electrons produced by 0.53 GeV/nucleon nitrogen and 10 GeV/nucleon iron nuclei in counter cell 3.5 cm from track (wire 6).

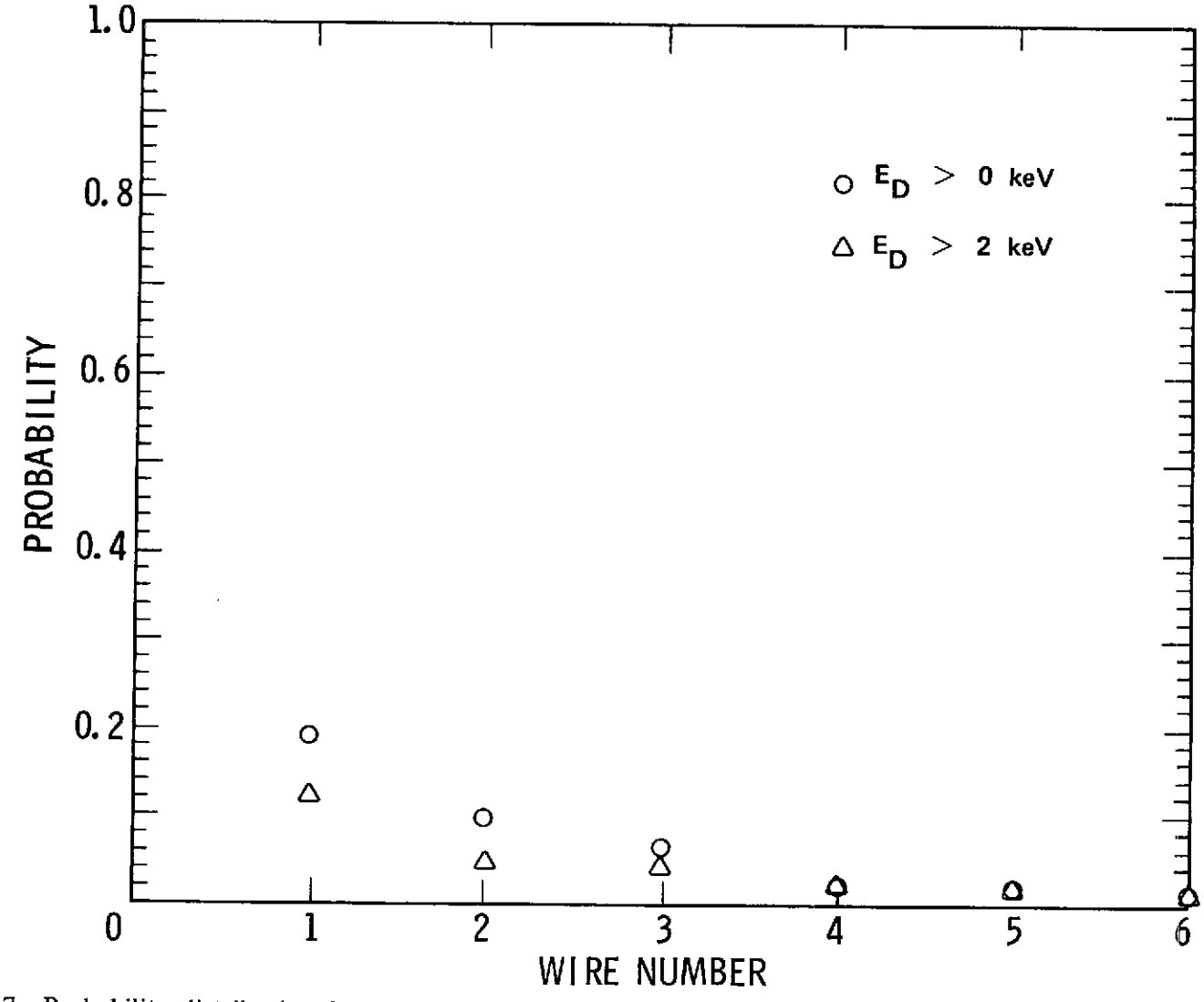

Figure A-7. Probability distribution for wires set by secondary electrons produced by 0.53 GeV/nucleon nitrogen nuclei (energy deposition of greater than 0 and 2 keV required to set a wire).

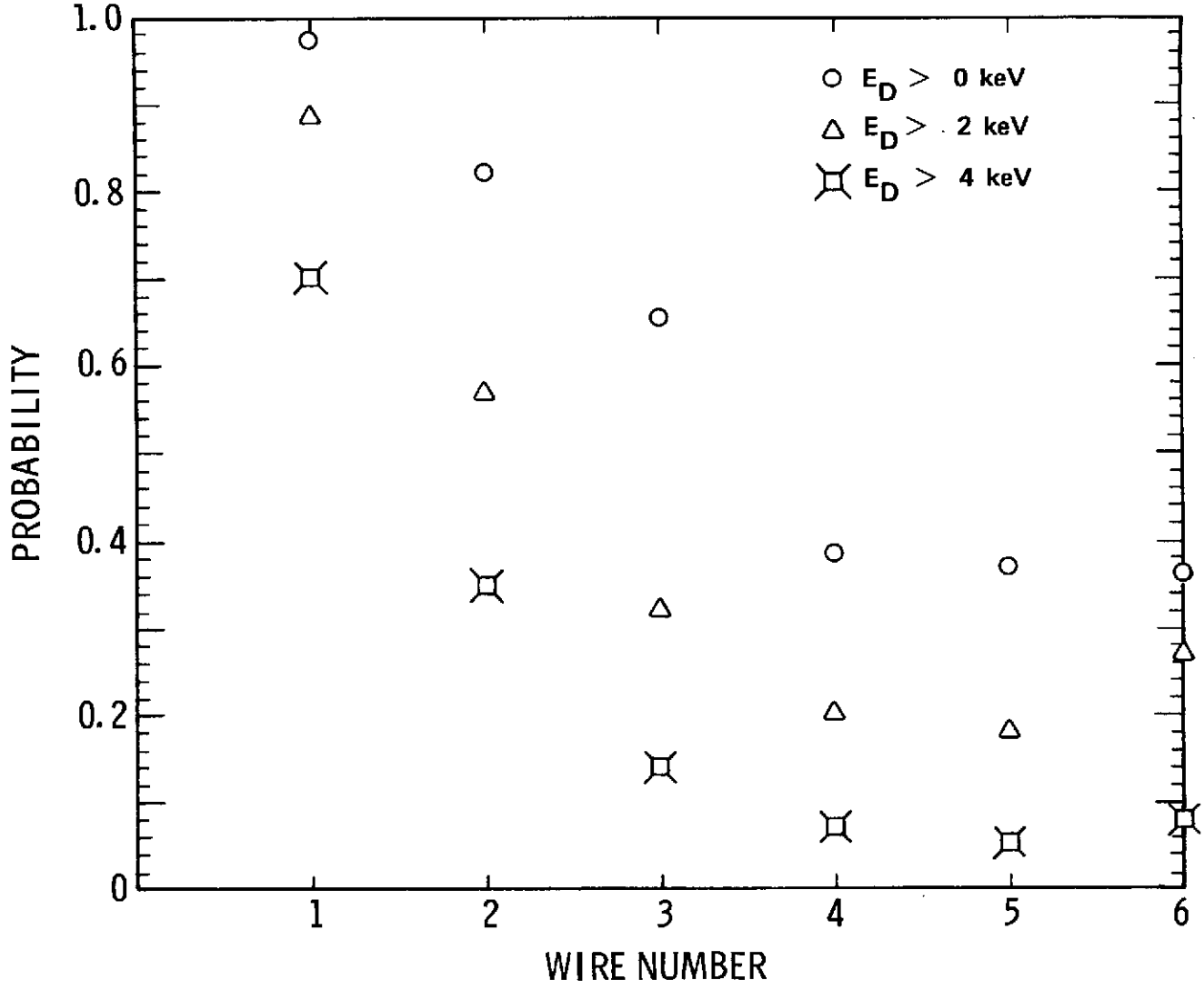

Figure A-8. Probability distribution for wires set by secondary electron produced by 10 GeV/nucleon iron nuclei (energy deposition of greater than 0, 2, and 4 keV required to set a wire).

REFERENCES

1. Charpak, G.: Ann. Rev. of Nucl. Sci., vol. 20, 1970, p. 195.

2. Eby, P. B.; and Morgan, S. H., Jr.: Phys. Rev., vol. A 5, 1972, p. 2536.

3. Morgan, S. H., Jr.; and Eby, P. B.: Nucl. Instr. and Meth., vol. 106, 1973, p. 429.

4. Sternheimer, R. M.: Phys. Rev., vol. 164, 1967, p. 349.

5. Uehling, E. A.: Ann. Rev. of Nucl. Sci., vol. 4, 1954, p. 315.

6. Vavilov, P. V.: Zh. Exper. Teor. Fiz., vol. 32, 1957, p. 320. Transl. JETP, vol. 5, 1957, p. 749.

7. Seltzer, S. M.; and Berger, M. J.: Studies in Penetration of Charged Particles in Matter. NAS-NCR Publication 1133, 1964.

8. Flammersfeld, A.: Naturw.,vol. 33, 1946, p. 280.

9. Berger, M. J.: Diffusion of Fast Charged Particles. Methods in Computational Physics, vol. 1, Academic Press, 1963.

10. Ormes, J. F.; et al.: Composition and Spectra of High Energy Cosmic Rays. NASA-GSFC X661-71-1 (N71-16602), Jan. 1971.

11. Rizzo, A.; et al.: IEEE Trans. on Nuclear Science, vol. NS-19, no. 3, 1972.

12. Austin, R. W.; et al.: Measurements of the Performance of Multiwire Proportional Chambers. NASA TN-D-7317, 1973.

13. Watts, J. W., Jr.: Calculation of Energy Deposition Distributions for Simple Geometries. NASA TN-D-7195, 1973.

14. Rossi, B.: High Energy Particles. Prentice-Hall, Englewood Cliffs, N.J., 1952, p. 31.

NASA-Langley, 1974